Eddy covariance data reveal that a small freshwater reservoir emits a substantial amount of carbon dioxide and methane

Alexandria G. Hounshell[1, †], Brenda M. D'Acunha[2], Adrienne Breef-Pilz[1], Mark S. Johnson[2,3], R. Quinn Thomas[1,4], Cayelan C. Carey[1]

[1]Department of Biological Sciences, Virginia Tech, Blacksburg, VA, USA, [2]Department of Earth, Ocean, and Atmospheric Sciences, University of British Columbia, Vancouver, BC, Canada, [3]Institute for Resources, Environment and Sustainability, University of British Columbia, Vancouver, BC, Canada, [4]Department of Forest Resources and Environmental Conservation, Virginia Tech, Blacksburg, VA, USA

Corresponding author: Alexandria G. Hounshell (alexgh@vt.edu)

† Current affiliation: National Centers for Coastal Ocean Science, National Oceanographic and Atmospheric Administration, Silver Spring, MD 20910, alexandria.hounshell@noaa.gov

Key Points:

- We measured high CO_2 (600 g C m^{-2} yr^{-1}) and CH_4 (1.0 g C m^{-2} yr^{-1}) annual fluxes, some of the first annual data from a small reservoir
- Carbon dioxide and methane fluxes exhibited statistically significant sub-daily, daily, weekly, and monthly timescales of variability
- Surface water temperature, dissolved oxygen, and fluorescent dissolved organic matter constrained reservoir fluxes on multiple timescales

Abstract

Small freshwater reservoirs are ubiquitous and likely play an important role in global greenhouse gas (GHG) budgets relative to their limited water surface area. However, constraining annual GHG fluxes in small freshwater reservoirs is challenging given their footprint area and spatially and temporally variable emissions. To quantify the GHG budget of a small reservoir, we deployed an eddy covariance system in a small (0.1 km^2) reservoir located in southwestern Virginia, USA for a full year to measure carbon dioxide (CO_2) and methane (CH_4) fluxes near-continuously. Fluxes were coupled with *in situ* sensors measuring multiple environmental parameters. Throughout the year, we found the reservoir to be a substantial source of CO_2 (~600 g CO_2-C m^{-2} yr^{-1}) and CH_4 (~1.0 g CH_4-C m^{-2} yr^{-1}) to the atmosphere, with significant sub-daily, daily, weekly, and approximately monthly timescales of variability. Importantly, we found annual GHG emissions estimated using eddy covariance were over an order of magnitude greater than diffusive GHG fluxes measured weekly to biweekly. During the winter, we found GHG fluxes during partial ice-on and open-water conditions were not statistically different, suggesting reservoirs may play an important role in freshwater GHG budgets throughout the year, not just during the open-water period. Finally, we identified several key environmental variables that may be driving GHG fluxes, specifically, surface water temperature and dissolved oxygen concentrations. Overall, our novel year-round eddy covariance data from a small reservoir indicate that these freshwater ecosystems likely contribute a substantial amount of CO_2 and CH_4 to global GHG budgets.

Plain Language Summary

Freshwater ecosystems have been shown to release substantial amounts of greenhouse gases, especially carbon dioxide and methane, to the atmosphere. Small waterbodies, such as lakes and reservoirs, are common in the landscape and may release particularly high levels of greenhouse gases, though their overall contribution remains unknown. The most common methods to date for estimating greenhouse gas emissions from freshwaters typically involve only measuring concentrations during the daytime on a handful of days throughout the year. Thus, there is a clear need for near-continuous measurements of carbon dioxide and methane from small waterbodies

throughout the year on multiple timescales (hours to months). To do this, we measured near-continuous fluxes of carbon dioxide and methane from a small reservoir using eddy covariance. We found this small reservoir to be a large source of both carbon dioxide and methane to the atmosphere over a full year and found high variability in fluxes measured at short (sub-daily) to long (seasonal) timescales. Overall, this study demonstrates the importance of small reservoirs as greenhouse gas sources to the atmosphere and emphasizes the need for additional measurements to estimate their contribution to global greenhouse gas budgets.

1 Introduction

Freshwater ecosystems play a disproportionately large role in global greenhouse gas (GHG) budgets relative to their total water surface area, often emitting more GHGs than are taken up by terrestrial ecosystems (Bastviken et al. 2011; Cole et al. 2007; DelSontro et al. 2018; Tranvik et al. 2009). Despite their importance, however, the contribution of inland waters remains under-represented within global carbon (C) and GHG budgets (Butman et al. 2018; Deemer and Holgerson, 2021; Deemer et al. 2016; DelSontro et al. 2018). To date, most studies measuring GHG emissions from freshwater lakes and reservoirs are based on snapshot measurements from short-term floating chamber deployments or grab samples of dissolved GHGs, which are extrapolated to broad spatial and temporal scales to estimate annual whole-ecosystem fluxes (Bastviken et al. 2015; Klaus et al. 2019; Wik et al. 2016). While these approaches have provided useful insights into general patterns of GHG cycling in freshwater ecosystems, they are inherently limited in capturing the high spatial and temporal variability in freshwater GHG fluxes (Baldocchi et al. 2021; Butman et al. 2018; Klaus et al. 2019; Rosentreter et al. 2021; Wik et al. 2016).

Among freshwater ecosystems, small (<1 km^2) reservoirs may be particularly under-represented in GHG budgets (Deemer and Holgerson, 2021; DelSontro et al. 2018; Rosentreter al. 2021). It is estimated that there are ~5.8 million lakes and reservoirs in the contiguous U.S. alone (Winslow et al. 2014), of which approximately half (~2.6 million) are human-made reservoirs (Smith et al. 2002). Small reservoirs (<1 km^2) compose >71% of reservoirs in the United States (National Inventory of Dams, USACE 2021), indicating that these ecosystems are

extremely common, with at least ~1.8 million small reservoirs in the conterminous U.S. However, constraining annual GHG estimates in small freshwater reservoirs is challenging given their small footprint area and heterogeneous GHG emissions (Loken et al. 2019; McClure et al. 2020; Podgrajsek et al. 2015). Short-term measurements indicate the potential for these ecosystems to exhibit high, but patchy fluxes (Deemer and Holgerson, 2021; DelSontro et al. 2018; McClure et al. 2018, 2020; Rosentreter et al. 2021), but to the best of our knowledge their annual emissions remain largely unknown.

Eddy covariance (EC) systems are increasingly being deployed on lakes and reservoirs to constrain sub-daily GHG fluxes on large spatial footprints, enabling the quantification of whole-ecosystem GHG fluxes at multiple temporal scales (e.g., Baldocchi et al. 2020; Golub et al. 2021; Eugster et al. 2011; Vesala et al. 2011; Waldo et al. 2021). EC systems are used to determine the net exchange of carbon dioxide (CO_2), methane (CH_4), and/or other gases at sub-hourly time scales via micrometeorology and *in situ* atmospheric trace gas concentrations measured using infrared gas analyzers (Baldocchi et al. 2020; Golub et al. 2021; Vesala et al. 2011). By collecting near-continuous data on the sub-hourly scale (typically measured at 20 Hz and reported as 30-minute means), EC systems allow GHG fluxes to be estimated at the sub-daily to annual timescales, improving our understanding of GHG flux temporal variability beyond traditional discrete measurements (Golub et al. 2021; Reed et al. 2018; Vesala et al. 2011). Additionally, EC systems often capture a larger spatial footprint compared to traditional discrete measurements, as measured fluxes represent the average flux from the atmospherically-mixed area upwind of the deployed EC system (Golub et al. 2021, Waldo et al. 2021). Thus, EC systems can greatly increase the temporal and spatial resolution of measured fluxes in lakes and reservoirs, with the caveat that important considerations and data filtering are needed for EC systems in small waterbodies. Specifically, a waterbody's small surface area decreases its EC footprint, both by increasing the likelihood of surrounding terrestrial vegetation impacting EC measurements of aquatic fluxes and decreasing the area available for a well-mixed, turbulent footprint (Esters et al. 2020; Vesala et al. 2011).

While the majority of reported freshwater EC studies have been conducted on short timescales (days to months; e.g., Erkkilia et al. 2018; Gorsky et al. 2021; Jammet et al. 2015; Podgrajsek et al. 2014, 2015; Vesala et al. 2006, 2011), longer-term studies measuring CO_2 or CH_4 fluxes in lakes and reservoirs on annual timescales are now becoming more common (e.g.,

Baldocchi et al. 2020; Golub et al. 2021; Jammet et al. 2017; Liu et al. 2016; Reed et al. 2018; Shao et al. 2015; Waldo et al. 2021). An annual study conducted in Lake Erie, USA found this highly-eutrophic system was a small sink of CO_2 during the summer productive season yet ultimately a CO_2 source on annual timescales (Shao et al. 2015). Other studies have highlighted the importance of short (hourly to daily), episodic events on annual CO_2 budgets, including the disproportionate effect of storms on annual CO_2 emissions from a large subtropical reservoir (Liu et al. 2016), fall mixing in a large (40 km^2) temperate lake (Reed et al. 2018), and pulses of CH_4 following ice-off in a north temperate lake (Gorsky et al. 2021). Seasonally, studies conducted during the winter found low and relatively consistent CO_2 fluxes during the ice-covered period (Baldocchi et al. 2020; Reed et al. 2018). In addition to noted diel, seasonal, and episodic variability in CO_2 fluxes, two annual studies recently found the sub-monthly timescale to be an important timescale of variability, though the mechanism for this variability remains unknown (Baldocchi et al. 2020; Golub et al. 2021).

Despite the increase in studies using EC systems to measure CO_2 and CH_4 fluxes from freshwaters, few studies to date have captured both CO_2 and CH_4 fluxes on the annual scale, especially during winter. Measuring annual-scale CO_2 and CH_4 fluxes is particularly important as GHG fluxes are rapidly changing due to altered climate (Bartosiewicz et al. 2019; Beaulieu et al. 2019). For example, increasing surface temperatures and changes in precipitation and nutrient loading are changing phytoplankton productivity and allochthonous C inputs to lakes and reservoirs (Fowler et al. 2020; Hanson et al. 2015; Tranvik et al. 2009). Changes in freshwater primary production and nutrient inputs to freshwater systems have been directly linked to changes in CO_2 (DelSontro et al. 2018), as well as CH_4 emissions (Deemer and Holgerson, 2021; DelSontro et al. 2018; McClure et al. 2020). Finally, increasing air temperatures are leading to warmer winters and more intermittent and partial ice cover (Imrit and Sharma, 2021; Sharma et al. 2021; Woolway et al. 2020), highlighting the need to understand the role of ice in constraining GHG fluxes. All these examples emphasize the importance of measuring near-continuous GHG fluxes on the annual scale with key environmental variables, such as precipitation and freshwater inflows, air and water temperature, chlorophyll-*a*, dissolved organic matter, and ice-on/ice-off as potential GHG drivers.

Altogether, there is a clear need to measure annual-scale CH_4 and CO_2 fluxes from small freshwater ecosystems, especially small reservoirs. To the best of our knowledge, only one

freshwater study has measured both CH_4 and CO_2 fluxes on an annual timescale (Jammet et al. 2017), while Waldo et al. (2021) measured only CH_4 fluxes at the annual scale. Waldo et al. (2021) used EC to measure annual CH_4 fluxes from a large (2.4 km^2), highly-eutrophic temperate reservoir, measuring emissions up to 71.4 g CH_4 m^{-2} yr^{-1}, which is in the top quarter of those reported to date from lakes and reservoirs. In an Arctic lake, Jammet et al. (2017) used EC to measure low GHG fluxes during ice cover, followed by large CH_4 and CO_2 fluxes during spring-thaw, and increasing ebullitive CH_4 fluxes during the ice-free season concurrent with high rates of CO_2 uptake due to photosynthesis. Aggregated across the full year, this Arctic lake was a net source of both CH_4 and CO_2 to the atmosphere (Jammet et al. 2017). Across the literature, most EC studies have focused on naturally-formed lakes, and all EC reservoir studies of which we are aware (Eugster et al. 2011; Golub et al. 2021; Liu et al., 2016; Waldo et al. 2021) were conducted in large (>2.4 km^2) reservoirs.

To better understand the GHG budgets of small reservoirs, we deployed an EC system in a small (0.1 km^2) freshwater reservoir located in southwestern Virginia, USA for a full year to measure CO_2 and CH_4 fluxes near-continuously. Flux measurements were coupled with *in situ* sensors measuring multiple environmental parameters, including surface water temperature, dissolved oxygen, chlorophyll-*a*, and fluorescent dissolved organic matter. We used the measured and gap-filled (i.e., modeled) GHG fluxes to answer the following three questions: 1) What is the annual phenology of CO_2 and CH_4 fluxes in a small, eutrophic reservoir, including during the critical winter period?; 2) What are the significant timescales of variability for CO_2 and CH_4 fluxes from hourly to seasonal timescales?; and 3) What environmental variables best explain CO_2 and CH_4 variability at hourly to monthly timescales?

2 Materials and Methods

2.1 Site description

Falling Creek Reservoir (FCR) is a small, eutrophic reservoir located in Vinton, Virginia, USA (Fig. 1; 37.30^{o}N, 79.84^{o}W; Howard et al. 2021). The reservoir and surrounding forested watershed are owned and operated by the Western Virginia Water Authority (WVWA) as a primary drinking water source (Gerling et al. 2016). FCR has a surface area of 0.119 km^2 and

maximum depth of 9.3 m (McClure et al. 2018). The reservoir is dimictic and thermally stratified from April to October (McClure et al. 2018). During the study period, water was not extracted for drinking water treatment and remained at a constant full-pond level.

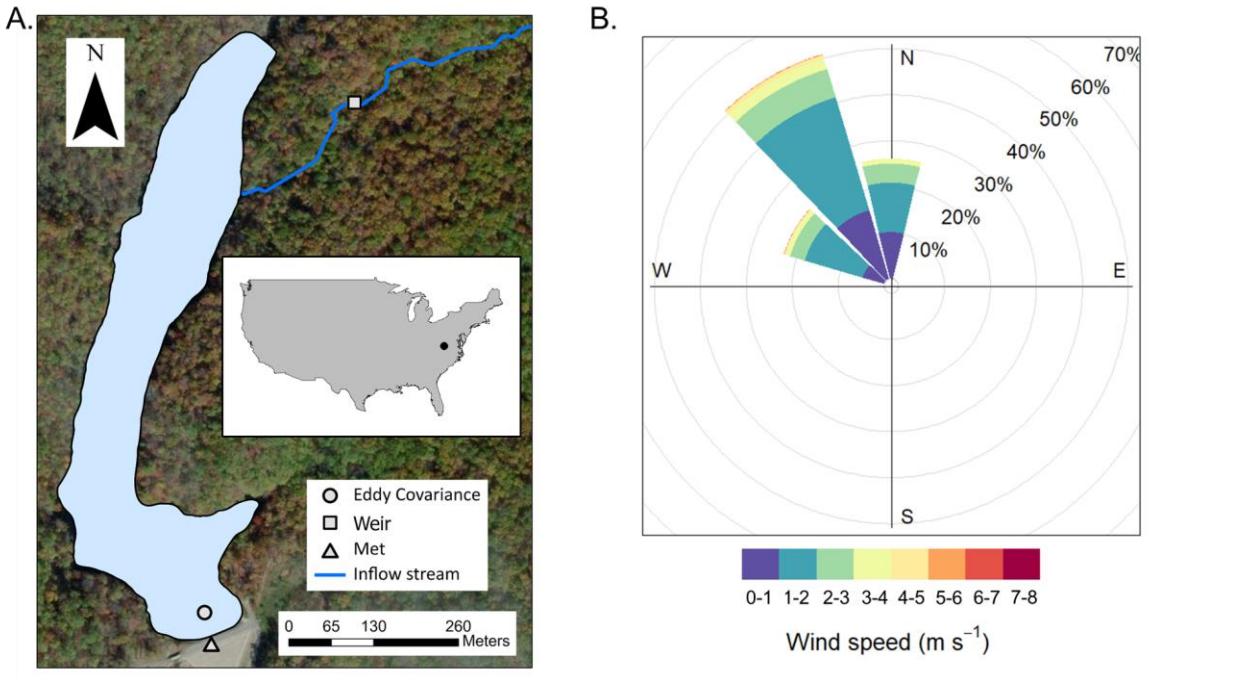

Figure 1. A. Map of Falling Creek Reservoir located in Vinton, Virginia, USA (map inset) showing location of the eddy covariance system, the weir located on the primary freshwater inflow, and the meteorological station located on the dam. B. Wind rose showing the dominant wind direction and wind speed (m s^{-1}) of greenhouse gas fluxes retained for analysis.

2.2 Data collection and overview

We used an EC system to measure CO_2 and CH_4 fluxes between the water surface and the atmosphere from 5 April 2020 to 6 April 2021 (details below; Carey et al. 2022a). To complement the EC measured fluxes, we also calculated CO_2 and CH_4 diffusive gas fluxes using dissolved CO_2 and CH_4 discrete grab samples collected during daylight hours (from 0800 to 1300) monthly to bimonthly from the water's surface at the deepest site of the reservoir (details below; Carey et al. 2022b).

In addition to the EC and diffusive fluxes, we also collected meteorological and environmental data. Briefly, a Campbell Scientific (Logan, Utah, USA) research-grade meteorological station measured air temperature; relative humidity; air pressure; wind speed and

direction; upwelling and downwelling shortwave and longwave radiation; total rainfall; photosynthetically-active radiation (PAR); and albedo every minute at the reservoir dam (sensor information provided by Carey et al. 2022c). At the reservoir's deepest site, we collected 10-minute water temperature measurements every 1 m from the surface (0.1 m) to just above the sediments (9 m) using a thermistor string. Thermistor data were used to calculate the difference in temperature between 0.1 m and 9.0 m (Diff. Temp) and daily buoyancy frequency (N^2), two metrics of thermal stratification, and thermocline depth throughout the study period (April 2020 to April 2021) using the LakeAnalyzer package in R (Winslow et al. 2016a). Fall turnover was defined as the first day in autumn when the temperature at 1 m was <1°C of the temperature measured at 8 m (1 November 2021; McClure et al. 2018).

Water column temperature data complemented 10-minute measurements of dissolved oxygen (DO) percent saturation, chlorophyll-*a* (Chl-*a*, µg L^{-1}), and fluorescent dissolved organic matter (fDOM, relative fluorescent units, RFU) measured using an EXO2 sonde (YSI, Yellow Springs, Ohio, USA) deployed at 1.6 m (Carey et al. 2022d). The EXO2 sonde was removed from the reservoir on 2 December 2020 for annual sensor maintenance and re-deployed on 27 December 2020. Finally, we measured stream inflow every 15 minutes on the primary inflowing stream to the reservoir via a gaged v-notch weir fitted with a Campbell Scientific CS451 pressure transducer (Campbell Scientific, Logan, Utah, USA), which was used to calculate the 15-minute flow rate following Carey et al. 2022e). The weir was breached on 20 July 2020 and repaired on 24 August 2020, resulting in no flow data during this interval.

2.3 Eddy covariance flux measurements

An EC system was deployed above the water surface over the deepest portion of the reservoir from 5 April 2020 to 6 April 2021. The EC instrumentation was installed on a permanent metal platform that extends ~45 m from the dam and 2.9 m over the reservoir's surface. As noted above, the reservoir was maintained at full pond, resulting in a consistent height of the EC system over the water's surface during the study period. The EC system included an ultrasonic anemometer to measure 3D wind speed and direction (CSAT3, Campbell Scientific), an open-path infrared gas analyzer for measuring CH_4 concentration (LI-7700, LiCor Biosciences, Lincoln, Nebraska, USA), and an enclosed-path infrared gas analyzer for measuring

CO_2 and water vapor concentrations (LI-7200, LiCor Biosciences), all recorded at 10 Hz by a data logger (LI-7550, LiCor Biosciences). On 10 August 2020, the data logger was removed for maintenance and re-deployed on 2 September 2020. Additionally, a thermocouple on the CO_2 sensor (LI-7500) was inoperable starting on 5 April 2021, terminating the EC time series.

The raw 10-Hz data were processed into 30-minute fluxes using the EddyPro v.7.0.6 software (LiCor Biosciences 2019). We conducted additional data processing following standard best practices, including: 1) removing wind directions which originated outside of the reservoir (80-250^o; Fig. 1); 2) removing extreme flux values (CO_2 fluxes $\geq |100|$ μmol C m^{-2} s^{-1}; CH_4 fluxes $\geq |0.25|$ μmol C m^{-2} s^{-1}); 3) removing CH_4 fluxes when the signal strength <20%; 4) removing CO_2 and CH_4 fluxes when they did not pass the test for stationarity or developed turbulent conditions (QC, quality control level 2 per Foken et al. 2004), in addition to when the latent heat flux (LE) or sensible heat (H) had QC level <2; 4) removing open-path CH_4 fluxes during periods of rainfall, which was determined based on the rain gage at the dam; 5) correcting for high-pass and low-pass filtering effects (Moncrieff et al. 2004); 6) removing additional periods of low turbulence friction velocity (u_*), as described below; and 7) removing data that corresponded to flux footprints that extended significantly beyond the reservoir.

We used REddyProc (Wutzler et al. 2021) to determine the u_* threshold for sufficiently turbulent conditions and removed any fluxes where u_* was < 0.081 m s^{-1}. To account for the uncertainty of estimating the u_* threshold, we used bootstrapping to estimate the distribution of u_* thresholds, and obtained the 5^{th}, 50^{th} and 95^{th} percentiles of this distribution (Wutzler et al., 2018). All the subsequent post-processing steps were repeated for each u_* scenario.

Flux footprints were modeled for each half-hour using a simple, two-dimensional parameterization developed by Kljun et al. (2015). This model builds on the Lagrangian stochastic particle dispersion model (Kljun et al. 2002), and provides information on the extent, width, and shape of the footprint. All the variables needed for the model were obtained directly from the dataset described above or calculated following Kljun et al. (2015). Fluxes were excluded when the along-wind distance providing the highest contribution (peak) to turbulent fluxes was outside the reservoir. All post-processing analyses were conducted using R statistical

software (v.4.0.3). Code for post-processing and all EC data can be found in the Environmental Data Initiative (EDI) repository (Carey et al. 2022a).

2.4 Eddy covariance gap-filling

Following the post-processing described above, we used the R package REddyProc (Wutzler et al. 2021) to conduct gap-filling to model missing flux data. First, we used the meteorological data measured at the dam to gap-fill any missing wind speed, direction, temperature, and relative humidity in the EC dataset (Table S1). Overlapping data show that all meteorological variables were tightly correlated between the EC system and the adjacent meteorological station (Pearson's rho=0.81-0.98; Table S1). Second, we calculated the vapor pressure deficit from measured air temperature and relative humidity and calculated net radiation balance from upwelling and downwelling shortwave and longwave radiation. Using REddyProc, we gap-filled all the remaining gaps in the data using the marginal distribution sampling (MDS) method, following Wutzler et al. (2018). Gap-filling was performed for each of the u_* scenarios, providing information about the uncertainty that might be introduced to the data by choosing a u_* threshold (step 6 above).

We note that power interruptions or instrument malfunction resulted in 79% and 60% raw data coverage for CO_2 and CH_4, respectively (Table S2). Ultimately, all data processing (filtering steps 1-7 described above) resulted in a total of 28% data coverage for CO_2 and 21% for CH_4 fluxes prior to gap-filling (Table S2), which is similar to previously-reported deployments of EC systems at lakes and reservoirs (e.g., Golub et al. 2021; Reed et al. 2018; Waldo et al. 2021). Comparisons of measured and gap-filled (modeled) EC data are in Fig. S1 and discussed below.

2.5 Diffusive flux measurements

We estimated discrete diffusive fluxes from FCR using dissolved CO_2 and CH_4 samples (Carey et al. 2022b) collected at the surface of the reservoir to compare with EC fluxes. Surface water samples were collected at 0.1 m depth using a 4-L Van Dorn sampler (Wildlife Supply Co., Yulee, Florida, USA) adjacent to the EC sensors (Fig. 1). Replicate (n=2) water samples were collected via a Van Dorn sampler into 20-mL serum vials without headspace, immediately capped, and then stored on ice until analysis within 24 hours. Samples were analyzed following

McClure et al. (2018) and Carey et al. (2022b) on a Shimadzu Nexis GC-2030 Gas Chromatograph (Kyoto, Japan) with a Flame Ionization Detector (GC-FID) and Thermal Conductivity Detector (TCD).

The measured surface samples were used to calculate CO_2 and CH_4 diffusive fluxes from the surface of FCR into the atmosphere on each day of sample collection following the equation:

$$\text{Flux} = k_{600} * (C_{surf} - C_{air}) \quad \text{Eq. 1}$$

where k_{600} is the gas transfer velocity (m d^{-1}) corrected for temperature and gas concentration (CO_2 or CH_4, respectively), C_{surf} is the concentration of CO_2 or CH_4 at the reservoir surface (0.1 m), and C_{air} is the atmospheric concentration of CO_2 or CH_4 measured by the EC system (Cole and Caraco, 1998). The k_{600} value was calculated every half-hour using multiple methods included in the LakeMetabolizer package in R (Cole and Caraco, 1998; Crusius and Wannikof 2003; Heiskanen et al. 2014; MacIntyre et al. 2010; Read et al. 2012; Soloviev et al. 2007; Vachon and Prairie, 2013; Winslow et al. 2016b, 2016). Mean half-hourly meteorological data used in k_{600} calculations were measured on FCR's dam (Carey et al. 2022c). Mean half-hourly surface water temperature was measured at the 0.1 m-deep thermistor deployed under the EC (Carey et al. 2022d). Both surface GHG replicates (n=2) were used to calculate fluxes; the resultant mean and standard deviation are reported.

2.6 Statistical analyses

To assess the phenology of fluxes (CO_2 and CH_4), we analyzed the mean and standard deviation (±1 S.D.) of EC fluxes at hourly, daily, weekly, and monthly time scales through the study period, which included both measured and gap-filled half-hourly fluxes. For both EC and discrete diffusive fluxes, negative fluxes correspond to fluxes into the reservoir (i.e., uptake) while positive fluxes are out of the reservoir (i.e., release to the atmosphere).

To assess diel variation in GHG fluxes, we compared median measured EC fluxes (i.e., not gap-filled) during the day (1100 to 1300) and night (2300 to 0100) throughout the year. As data were not normally distributed, we used paired Wilcoxon signed-rank tests to assess statistical significance of paired day-night fluxes. Additionally, we compared dawn (0500 to

0700) and dusk (1700 to 1900) median EC measured fluxes using the same methods. All time periods (i.e., day and night; dawn and dusk) were held constant throughout the year.

Ice coverage at FCR is episodic and ephemeral, encompassing longer ice-covered periods as well as shorter-duration ice-covered periods when ice may be present during portions of sequential days or with partial coverage of the reservoir's surface, which we refer to as intermittent ice-on periods. To explore the role of winter intermittent ice cover on CO_2 and CH_4 fluxes, we plotted mean hourly fluxes (±1 S.D.) from 24 December 2020 to 11 February 2021, which encompassed two periods of partial ice-on and two periods of complete ice-off (following Carey 2021; Table S3). We removed the final intermittent ice-on period during late February 2021 due to lack of measured EC data. We used Mann-Whitney-Wilcoxon tests to determine statistically-significant differences ($\alpha = 0.05$) between median half-hourly fluxes measured during intermittent ice-on and complete ice-off (i.e., open-water) periods.

Finally, we calculated the net annual flux balance for CO_2 and CH_4 estimated using both the half-hourly EC data (measured and gap-filled) and measured discrete diffusive fluxes. Fluxes from both methods were summed across the entire yearlong study period (5 April 2020 to 6 April 2021). For the discrete diffusive fluxes, we used the mean of all k_{600} methods (Cole and Caraco, 1998; Crusius and Wannikof 2003; Heiskanen et al. 2014; MacIntyre et al. 2010; Read et al. 2012; Soloviev et al. 2007; Vachon and Prairie, 2013; Winslow et al. 2016). The standard deviation (±1 S.D.) was calculated for the measured and gap-filled data and for the diffusive flux data using the two grab sample replicates and all k_{600} methods.

2.7 Time series analysis

To determine dominant time scales of variability in the EC flux data (measured and gap-filled), we conducted Morlet continuous wavelet transforms (CWTs; Carey et al. 2016; Howard et al. 2021; Torrence and Compo, 1998). CWTs identify the relative importance of different time frequencies throughout the time series using a scaled oscillating function and outputs different power function values for each time scale and sampling interval (Carey et al. 2016; Howard et al. 2021; Torrence and Compo, 1998). Following the Nyquist theorem, we determined the importance of different time scales ranging from one hour to six months, representing twice the timescale of our sampling interval (half-hourly) to half the timescale of our full time series (1

year; Nyquist, 1928; Shannon, 1949). We conducted separate Morlet CWTs on normalized (z-score) gap-filled CO_2 and CH_4 fluxes (Torrence and Compo, 1998), focusing on the interpretation of results outside the cone of influence (COI), which shows where edge effects may distort results, especially at longer time scales (Carey et al. 2016; Howard et al. 2021; Torrence and Compo, 1998). We used a 95% confidence interval to compare the coefficients from the power spectra to coefficients from a red-noise spectrum to determine the significance of each time scale (Carey et al. 2016). Finally, we calculated the global power spectrum for the time series by averaging the power function values for each time scale across the study period, which was used to determine the dominant time scale of variability (following Carey et al. 2016). CWT analysis was conducted using the dplR R package (Bunn et al. 2020).

To identify key environmental predictors of the observed mean hourly, daily, weekly, and monthly CO_2 and CH_4 fluxes (measured and gap-filled), we developed separate autoregressive integrated moving average (ARIMA) models for each time scale. ARIMA models are used to identify key environmental predictors while accounting for temporal autocorrelation (Hyndman and Athanasopoulos, 2018). We selected several potential environmental predictors, including: surface water temperature (Temp, 0.1 m, ^{o}C); Diff. Temp; buoyancy frequency (N^2); thermocline depth (TD); DO percent saturation (DO sat); Chl-*a*; fDOM; and discharge (Inflow) measured at the primary inflow to FCR (Fig. S2). Prior to ARIMA modeling, we conducted pairwise Spearman correlations on all predictor variables (aggregated to each scale) and removed collinear variables (Pearson's rho$\geq$0.7) that were the least correlated with fluxes. N^2 and Diff. Temp were removed for all time scales due to their strong correlation with surface temperature (Table S4). At the monthly timescale, Inflow and fDOM were removed (Table S4). Response and predictor variables were checked for skewness, transformed if appropriate, and normalized (z-scores) prior to model fitting (Hounshell et al. 2022).

We used a model selection algorithm (Lofton et al. 2021) to identify the importance of environmental predictor variables. The algorithm was based on the auto.arima function in the forecast package in R (Hyndman and Khandakar, 2008; Hyndman et al. 2021) which compared fitted models to a global model (all possible predictors) and a null persistence model with just one autoregressive term (AR(1)). We selected the environmental model with the lowest corrected Akaike information criterion (AICc), as well as models within 2 AICc units (Burnham and

Anderson, 2002). Models were limited to include one autoregressive term (Hounshell et al. 2022).

3 Results

3.1 Phenology of CO_2 and CH_4 fluxes

High-frequency EC time series (measured and gap-filled) data show that FCR was generally a net source of both CO_2 and CH_4 to the atmosphere throughout the year-long study period, with substantial variability at the hourly, daily, weekly, monthly, and seasonal scales (Figs. 2, S3, S4; Tables S5, S6). At the hourly scale, mean CO_2 fluxes ranged from -29.14 to 39.19 μmol m^{-2} s^{-1} with a mean hourly flux of 1.66 ± 4.25 μmol m-^{2} s^{-1} (±1 S.D.) as aggregated over the year. Mean hourly CH_4 fluxes ranged from -0.0479 to 0.0750 μmol m^{-2} s^{-1} with a mean hourly CH_4 flux of 0.0027 ± 0.0071 μmol m^{-2} s^{-1} (Fig. S3; Table S6). At the daily scale, mean CO_2 fluxes ranged from -4.16 to 11.80 μmol m^{-2} s^{-1} with a mean flux of 1.66 ± 2.07 μmol m^{-2} s^{-1}, and -0.0078 to 0.0188 μmol C m^{-2} s^{-1} for CH_4 with a mean flux of 0.0027 ± 0.0043 μmol m^{-2} s^{-1} (Fig. 2; Tables S5, S6).

Diel comparisons between measured (i.e., not gap-filled) EC fluxes reveal significantly higher measured CO_2 fluxes during the day (1100 to 1300) as compared to night (2300 to 0100; p=0.02; Fig. 3; Table S7), but no statistically significant difference between measured day and night CH_4 fluxes (p=0.43; Fig. 3; Table S7). The difference between median day-night CO_2 fluxes was 0.38 μmol m^{-2} s^{-1} and ranged up to 2.19 μmol m^{-2} s^{-1} in summer. Importantly, wind speed was also significantly greater (0.20 m s^{-1}) during the day as compared to night (p<0.001; Fig. 3; Table S7), which likely explains higher daytime fluxes (following Cole and Caraco, 1998). We also observed significantly higher median CO_2 fluxes measured at dawn (0500 to 0700; 1.31 μmol m^{-2} s^{-1}) as compared to dusk (1700 to 1900; 0.11 μmol m^{-2} s^{-1}; p<0.001; Fig 3; Table S7) and higher median dawn wind speeds (p<0.001). For CH_4, there was no statistical difference between dawn and dusk fluxes.

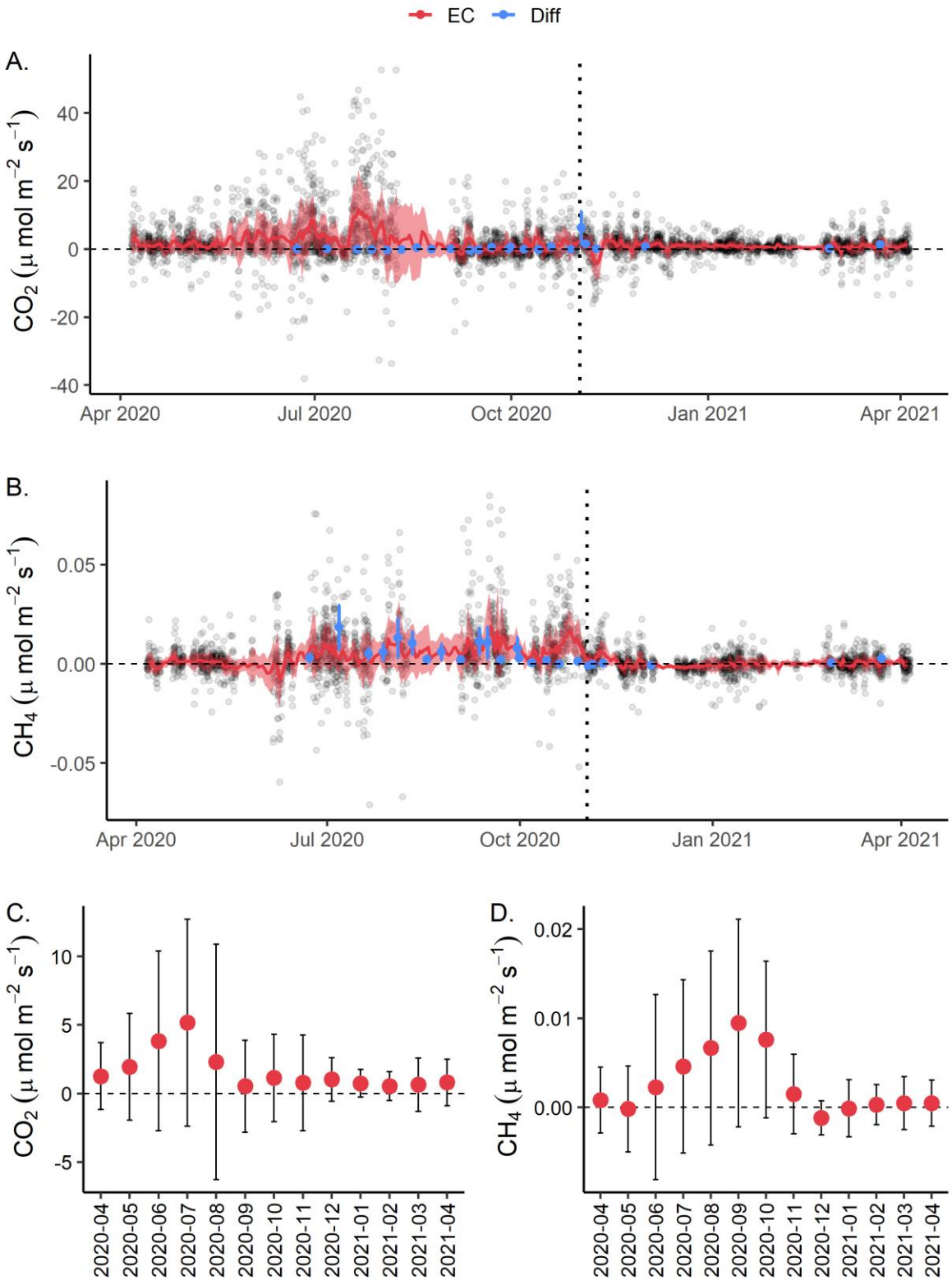

385

386 **Figure 2.** A. Daily mean carbon dioxide fluxes (CO_2, μmol m^{-2} s^{-1}) and B. daily mean methane
387 fluxes (CH_4, μmol m^{-2} s^{-1}) measured from April 2020 to April 2021 using eddy covariance (EC,

red) and calculated discrete diffusive fluxes (Diff, blue) using the mean and standard deviation of multiple gas transfer coefficient models (k_{600}; Winslow et al. 2016b). Grey dots represent measured half-hourly fluxes from the EC. The dark red line represents daily mean fluxes, including gap-filled time points. The shaded red area represents ±1 standard deviation of the daily 30-minute fluxes using both measured and gap-filled EC fluxes. The vertical dotted line indicates reservoir fall turnover. C. Mean monthly CO_2 fluxes (μmol m^{-2} s^{-1}) and D. Mean monthly CH_4 fluxes (μmol m^{-2} s^{-1}) aggregated from measured and gap-filled EC data. The error bars correspond to ±1 S.D. of aggregated fluxes for both measured and gap-filled EC values. The horizontal dashed line indicates zero fluxes.

Hourly CO_2 diffusive fluxes calculated from grab surface samples were an order of magnitude lower than EC fluxes and ranged from -1.65 to 35.96 μmol m^{-2} s^{-1}, with a mean flux of 0.38 ± 0.92 μmol m^{-2} s^{-1} (Figs. 2, S5; Table S5, mean diffusive fluxes). The magnitude of diffusive fluxes was highly sensitive to the gas transfer coefficient method (k_{600}) used in flux calculations (Eq. 1). Varying the gas transfer coefficient method led to a range of mean hourly CO_2 fluxes from 0.18 μmol m^{-2} s^{-1} (Crusius method; Crusius and Wannikof, 2003) to 0.95 μmol m^{-2} s^{-1} (MacIntyre method; MacIntyre et al. 2010; Table S5; Fig. S5). Hourly CH_4 diffusive fluxes were more comparable to measured EC fluxes, with a range of -0.0059 to 0.0928 μmol m^{-2} s^{-1} and a mean of 0.0048 ± 0.0074 μmol m^{-2} s^{-1} (Figs. 2, S5; Table S6, mean diffusive fluxes). For CH_4, different gas transfer coefficients led to a range of 0.0018 μmol m^{-2} s^{-1} (Crusius method; Crusius and Wannikof, 2003) to 0.0121 μmol m^{-2} s^{-1} (MacIntyre method; MacIntyre et al. 2010; Figs. S6, S7 Table S6). For both CO_2 and CH_4, diffusive fluxes were within the range of measured and gap-filled EC fluxes (Fig. 2; Table S6).

At the seasonal scale, both CO_2 and CH_4 fluxes were greater in magnitude and more variable during the summer than winter (Fig. 2). During the summer months (June – August), FCR was an overall source of CO_2 and CH_4 to the atmosphere (Fig. 2). There were particularly high CO_2 fluxes from FCR during July 2020 and high CH_4 fluxes in late summer (July – August; Fig. 2). FCR was a small CO_2 sink immediately following reservoir turnover (i.e., mixing due to surface cooling) in October 2020, while CH_4 fluxes declined but remained positive immediately following turnover. From September to April, FCR was a small CO_2 source, but emitted less CO_2 than during the summer. For CH_4, FCR was almost net neutral from late fall to early spring (November to April), especially compared to larger CH_4 emissions during the summer. We note that comparisons between measured and gap-filled (modeled) EC fluxes suggest that the gap-filled method used in this study likely underestimated total CO_2 and CH_4 fluxes (Fig. S1). Thus,

the EC fluxes presented in this study are likely a conservative estimate of FCR's total contribution of GHGs to the atmosphere.

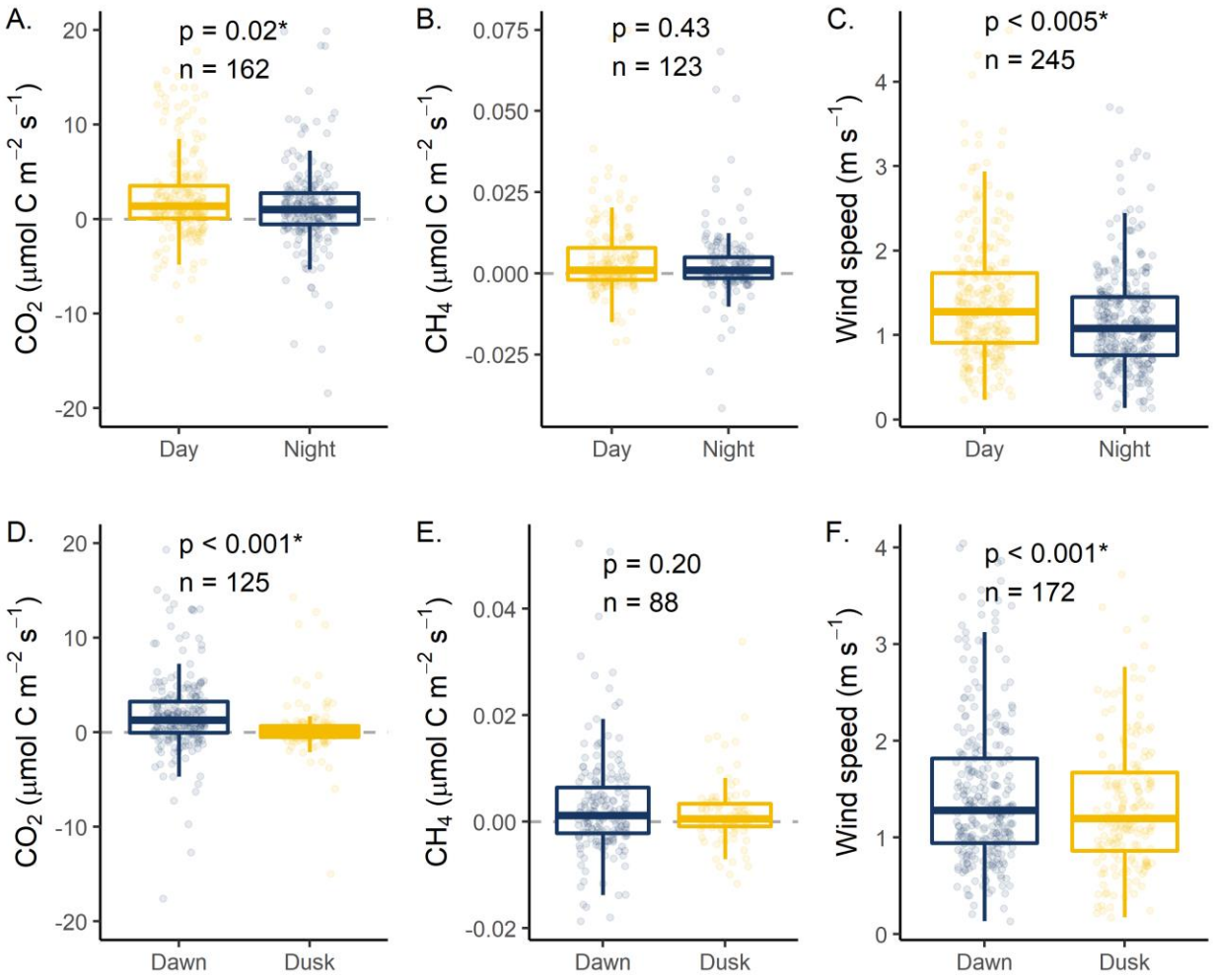

Figure 3. Diel (day versus night) comparisons of A. carbon dioxide (CO_2, µmol m^{-2} s^{-1}), B. methane (CH_4, µmol m^{-2} s^{-1}), and C. wind speed (m s^{-1}) measured using the eddy covariance (EC) system deployed at Falling Creek Reservoir. Points represent the median flux calculated for each day (1100 to 1300) and night (2300 to 0100) when measured EC data were available. Dawn (0500 to 0700) versus dusk (1700 to 1900) comparisons of D. CO_2, E. CH_4, and F. wind speed. Wilcoxon sign-ranked tests were used to determine statistical significance between paired (day to night; dawn to dusk) measurements. Statistical significance was defined a priori as $p<0.05$; asterisks indicate statistically significant differences. n indicates the number of paired measurements (Table S7). For CO_2 (A. and B.) some outliers were omitted for data presentation but retained for analysis.

3.2 Influence of intermittent, partial ice cover on CO_2 and CH_4 fluxes

Throughout the winter period, CO_2 and CH_4 mean fluxes were much lower than in the summer, with small to no differences in fluxes between the intermittent ice-on or ice-off winter periods (Fig. 2). When aggregating measured half-hourly fluxes across each ice-on and ice-off period, there was no statistically-significant difference between median CO_2 and CH_4 fluxes measured during complete ice-off vs. intermittent ice-on for either the first or second ice-on/ice-off periods (Kruskal-Wallis p>0.05; Fig. 4; Table S8).

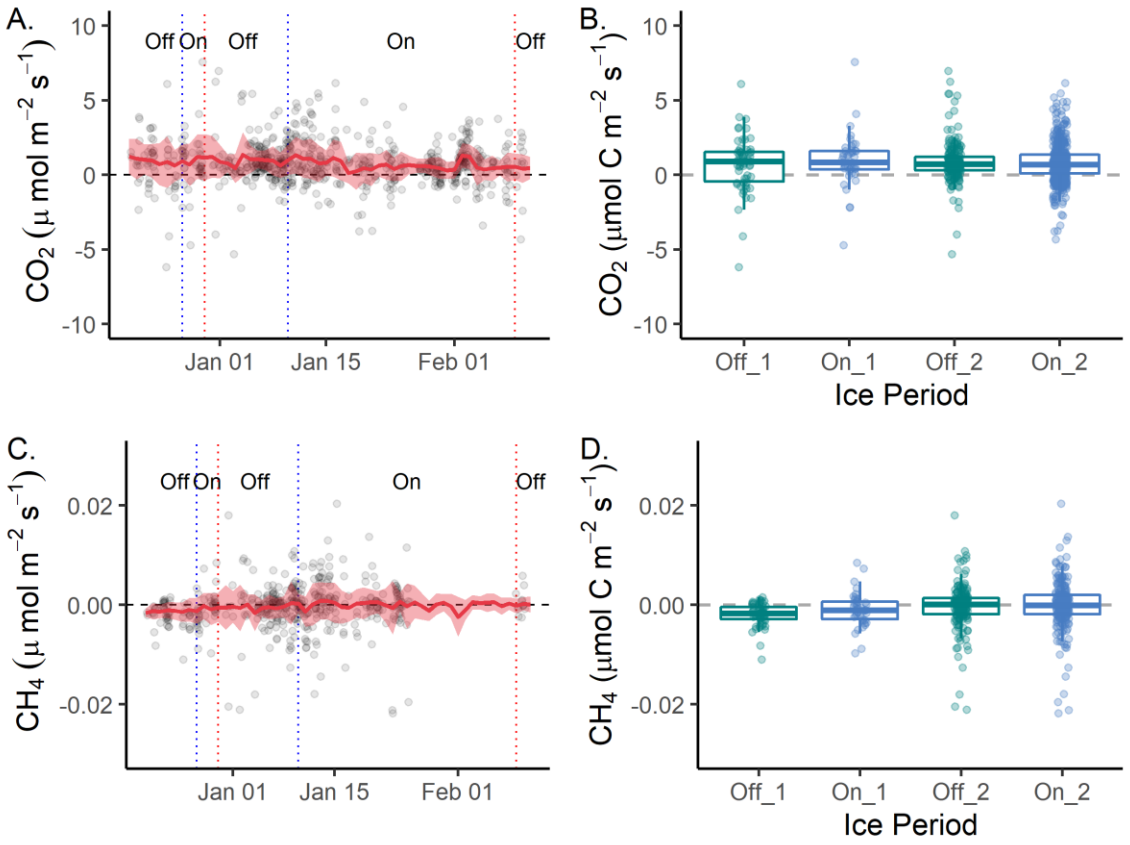

Figure 4. Mean daily fluxes during the winter for A. Carbon dioxide fluxes (CO_2, μmol m^{-2} s^{-1}) and C. Methane fluxes (CH_4 μmol m^{-2} s^{-1}) during sequential partial ice-on ("On") and complete ice-off ("Off") periods at Falling Creek Reservoir. Grey dots represent measured half-hourly fluxes while the solid red line indicates mean daily fluxes. The shaded red area corresponds to the standard deviation (±1 S.D.) of the daily mean fluxes. The blue vertical dashed lines correspond to partial ice-on while the red vertical dashed lines correspond to complete ice-off. Boxplots of measured B. CO_2 and D. CH_4 fluxes during each ice-on and ice-off period. For each box plot, the median is represented as the bold line while the 25th and 75th percentiles are represented as the bottom and top of the box, respectively. The whiskers represent minimum and maximum values (1.5× interquartile range). Points represent all half hourly fluxes measured

separated by each ice-on and ice-off period. The dashed horizontal line corresponds to zero fluxes.

3.3 Dominant timescales of variability

CWT analysis identified several important timescales of variability for both CO_2 and CH_4 fluxes, including: sub-daily (12 hour), daily (1 day), weekly (7 days), and approximately monthly (hereafter, monthly) (Figs. 5, S8). Overall, the monthly timescale was the most dominant timescale of variability for both CO_2 and CH_4 fluxes, as determined by the global power spectrum aggregated across the entire time series (Fig. 5), and most likely to be a statistically-significant timescale during the summer, fall, and winter. The weekly timescale was also a significant timescale of variability for both GHGs during the summer and fall. In comparison, the daily and subdaily timescales were less consistently important for both fluxes. Over the year-long study, 76 days exhibited significant variability at the daily timescale for CO_2 and 82 days for CH_4, both mainly in the summer, while the sub-daily scale was important for CO_2 on 34 days and CH_4 on 34 days during the summer (Fig. S9).

3.4 Environmental predictors of CO_2 and CH_4 fluxes

Overall, surface water temperature was found to be the most important environmental predictor for both CO_2 and CH_4 fluxes over all timescales (hourly, daily, weekly, monthly), followed by DO sat (Table 1). Chl-*a*, fDOM, and inflow were only intermittently important for CO_2 and CH_4 fluxes at various timescales (Tables 1, S9). Both temperature and DO sat were negatively correlated with CO_2 at the hourly timescale, but positively correlated at the daily, weekly, and monthly timescales. CO_2 fluxes were negatively associated with Chl-*a* at the daily timescale while CO_2 was positively correlated with fDOM at the hourly, daily, and weekly timescales. Inflow was positively correlated with CO_2 fluxes, but only at the daily timescale. Across all timescales, the best-fitting ARIMA model for CO_2 was identified at the monthly timescale (RMSE=0.33 μmol m^{-2} s^{-1}), with descending RMSE for the daily, weekly, and hourly models ranging from 0.47-0.74 μmol m^{-2} s^{-1} (Tables 1; S8).

Similar to CO_2, CH_4 fluxes were correlated with surface water temperature at all timescales followed by DO sat, with negative correlations with temperature at the hourly timescale and positive correlations with temperature at the daily, weekly, and monthly

timescales. At the hourly and monthly timescales, CH_4 was negatively correlated with DO sat, and negatively correlated with inflow at the weekly timescale. Contrary to CO_2, CH_4 fluxes were positively correlated with Chl-*a* at the daily timescale and fDOM was not identified as an important environmental predictor at any timescale. Overall, the best-fitting ARIMA model was identified at the daily timescale (RMSE=0.45 µmol m^{-2} s^{-1}) with descending RMSE for the monthly, weekly, and hourly models ranging from 0.51-0.73 µmol m^{-2} s^{-1} (Tables 1, S9). Full ARIMA results are reported in Table S9.

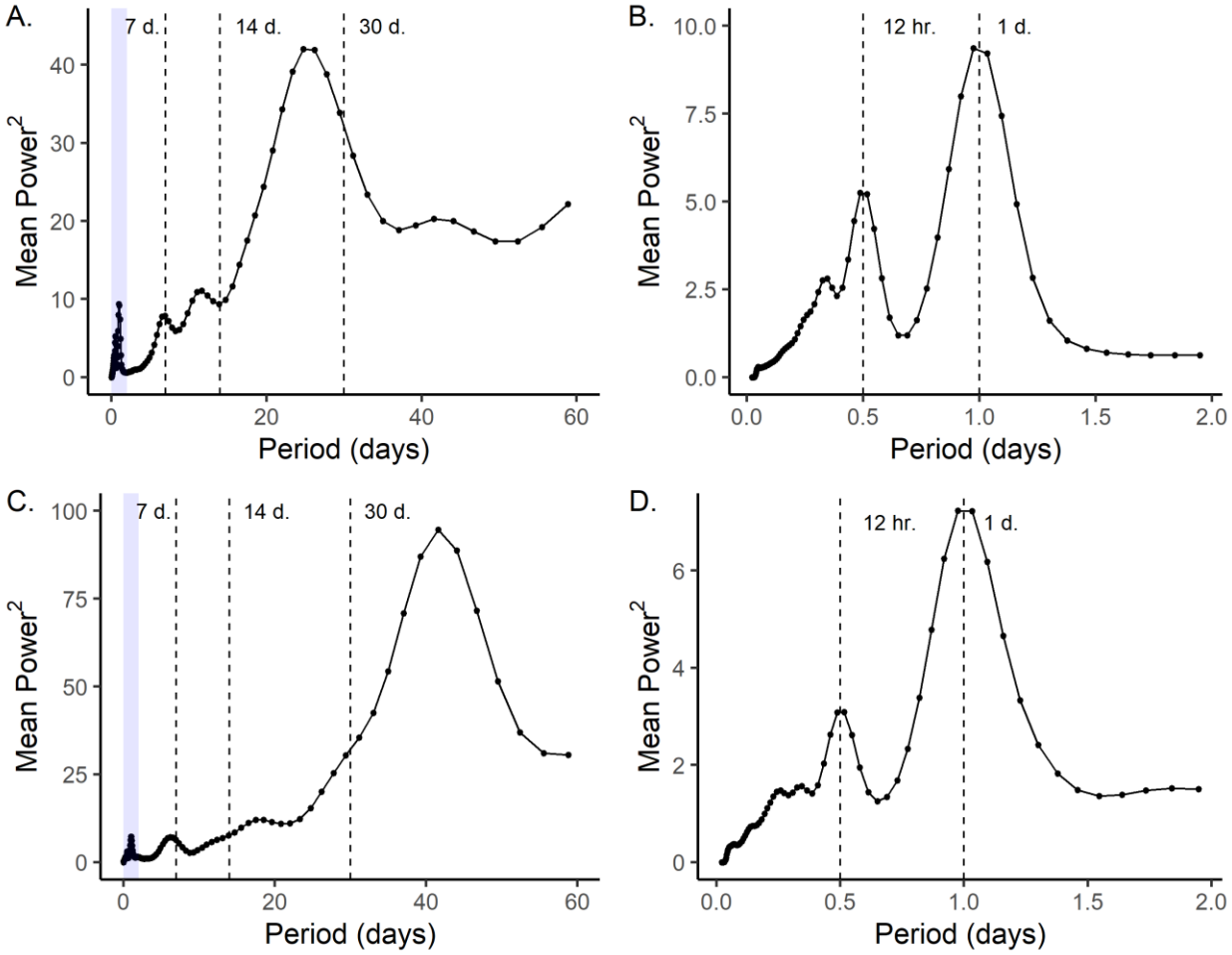

Figure 5. Mean global power spectra showing dominant time scales of variability for the entire time series of A. carbon dioxide fluxes (CO_2, µmol m^{-2} s^{-1}) and C. methane fluxes (CH_4, µmol m^{-2} s^{-1}), as identified in continuous wavelet transforms (CWTs) and truncated to 60 days. The purple box in A. and C. indicates the half-hour to two-day timescale expanded in panel B. for CO_2 and D. for CH_4 fluxes. Vertical dashed lines indicate significant time scales (30 days, 14 days, 7 days, 1 day, and 12 hours) throughout the 60-day time period. The CWTs are shown in Figure S8.

Table 1. *Best-fit results from Autoregressive Integrated Moving Average (ARIMA) analysis*

GHG	Timescale	Model Order	Surface Temp (°C)	DO Sat. (%)	Chl-a (µg L^{-1})	fDOM (RFU)	Inflow (m^3 s^{-1})	Thermo. Depth (m)	RMSE (µmol m^2 s^{-1})
CO_2	Hourly	(0,1,4)	-0.72	-0.09	-	0.07	-	-	0.74
	Daily	(0,0,4)	0.30	0.17	-0.16	0.14	0.21	-	0.47
	Weekly	(0,0,0)	0.21	0.59	-	0.30	-	-	0.55
	Monthly	(0,0,0)	0.40	0.68	-	x	x	-	0.33
CH_4	Hourly	(1,1,3)	-0.29	-0.04	-	-	-	-	0.73
	Daily	(1,0,3)	0.48	-	0.14	-	0.00	-	0.45
	Weekly	(0,0,1)	0.56	-	-	-	-0.34	-	0.56
	Monthly	(0,0,0)	0.97	-0.54	-	x	x	-	0.51

Note: Table includes only the top selected model (lowest corrected Akaike Information Criterion, AICc) which included at least one environmental predictor. Models are separated by greenhouse gas (GHG) flux as carbon dioxide (CO_2) and methane (CH_4) as well as by timescale (hourly, daily, weekly, monthly). Environmental predictors included: Surface temperature (Surface Temp, °C), dissolved oxygen saturation (DO Sat, %), Chlorophyll-*a* (Chl-*a*, µg L^{-1}), fluorescent dissolved organic matter (fDOM, RFU), inflow discharge (Inflow, m^3 s^{-1}), and thermocline depth (Thermo. Depth, m). Model order is specified as (p,d,q) where p is the order of the AR term, d is the order of the integration term, and q is the order of the MA term. For brevity, the autoregressive (AR) and moving average (MA) terms have been removed but can be found in the supplemental information. Results for all models with 2 AICc of the best fitting model, can be found in the supplemental information (Table S9). Dashed lines indicate environmental parameters that were not identified as statistically significant. X's indicate environmental variables which were removed prior to modeling due to collinearity (Pearson's rho>|0.70|). The root mean square error (RMSE) is reported for each model. Standard errors for each parameter value are given in Table S9.

3.5 Net CO_2 and CH_4 balance for a small, eutrophic reservoir

CO_2 and CH_4 fluxes summed across the entire year indicate that FCR is an overall source of CO_2 and CH_4 to the atmosphere. According to EC fluxes, FCR released 630 g CO_2-C m^{-2} and 1.02 g CH_4-C m^{-2} for the entire year. This annual GHG balance was driven by large fluxes of CO_2 and CH_4 during the summer, as CO_2 and CH_4 fluxes were 3× and 23× greater, respectively, during the summer stratified period (April – October) as compared to the winter and early spring (November – March; Fig. 6). Net emissions during the warmest months (June – September, 376 g CO_2-C m^{-2}) represented 61% of the total annual net CO_2 flux as compared to the coldest months (December – March) when only 60 g CO_2-C m^{-2} was emitted (9.3% of the total annual CO_2). Similarly, for CH_4, 72% of the total annual net CH_4 flux was released during the warmest months (June – September) and only 2.5% during the coldest months (December – March; 0.73 and 0.02 g CH_4-C m^{-2}). Cumulatively, the amount of CO_2-C released from FCR was three orders of magnitude greater than the mass of CH_4-C released.

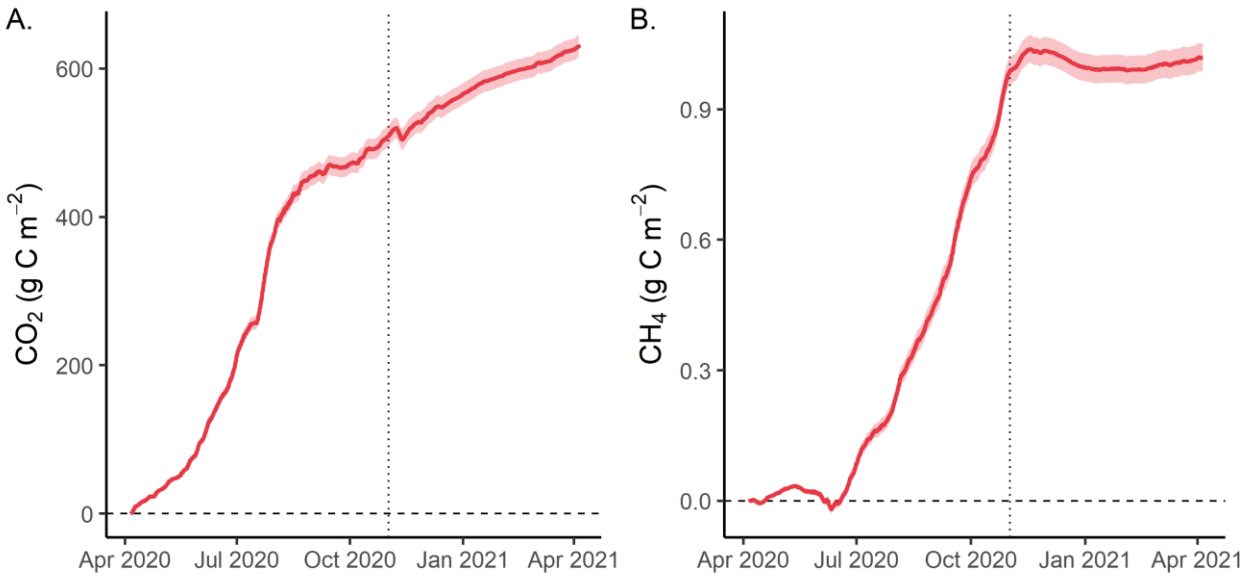

Figure 6. Annual cumulative fluxes for A. carbon dioxide (CO_2, g C m^{-2}) and B. methane (CH_4, g C m^{-2}) using gap-filled eddy covariance fluxes from Falling Creek Reservoir. Shaded areas correspond to the aggregated standard deviation (±1 S.D.) of measurements. The horizontal dashed line corresponds to zero and the vertical dotted line indicates reservoir fall turnover.

4 Discussion

This study provides the first annual-scale estimates of CH_4 and CO_2 fluxes using an EC system from a small reservoir and indicates that GHG emissions from small freshwater waterbodies may be substantially underestimated compared to past studies. Importantly, FCR had an order of magnitude lower net annual CH_4 fluxes but 6× higher net annual CO_2 fluxes per area than the mean of previous estimates of CH_4 and CO_2 fluxes from reservoirs around the world (mean 43.8 g CH_4-C m^{-2} yr^{-1}; 120.5 g CO_2-C m^{-2} yr^{-1}; Deemer et al. 2016). Even compared to more recent EC studies, FCR was a smaller source of CH_4 (30 - 64 g CH_4-C m^{-2} yr^{-1}; Waldo et al. 2021), yet a much larger source of CO_2 (-53.6 – 164.7 g CO_2-C m^{-2} yr^{-1}; Baldocchi et al. 2020; Golub et al. 2021) to the atmosphere. Altogether, our work reveals substantial variability in both CH_4 and CO_2 fluxes over sub-daily to seasonal scales and underscores the need for more accurately quantifying the GHG contributions of small reservoirs on multiple timescales.

4.1 Substantial variability in sub-daily fluxes, with higher day than night CO_2 fluxes

A key advantage of an EC system is the ability to capture variability in sub-daily GHG fluxes throughout the year. Our continuous wavelet transform (CWT) analysis identified the sub-daily (12-hour) timescale as an important timescale of variability for both CO_2 and CH_4 fluxes, especially in the summer (Figs. S8, S9). Our work complements previous studies of freshwater systems using EC measurements that observed high sub-daily variability in both summer CO_2 (Liu et al. 2016; Golub et al. 2021; Shao et al. 2015) and CH_4 fluxes (Eugster et al. 2011; Podgrajsek et al. 2014; Waldo et al. 2021).

We observed significantly higher CO_2 fluxes during the day as compared to night (Fig. 3A), but no diel differences in CH_4 fluxes using measured EC fluxes aggregated over the full year (Fig. 3B). Previous studies have also observed diel patterns in GHG fluxes: e.g., some lake and reservoir studies have shown higher CH_4 fluxes observed during the night (Eugster et al. 2011; Podgrasjek et al. 2014; Waldo et al. 2021) and higher CO_2 fluxes at night in streams (Attenmeyer et al. 2021; Gómez-Gener et al. 2021). Other studies, however, have found a positive relationship between CH_4 fluxes and surface water temperature at the half-hourly timescale, which results in higher CH_4 fluxes during the day as compared to night (Erkkilia et al. 2018; Jammet et al. 2017; Podgrasjek et al. 2016). We hypothesize that statistically higher wind

speeds during the day at FCR (Fig. 3C) likely resulted in higher observed CO_2 fluxes measured by the EC due to higher piston velocities, leading to more effective daytime gas transfer (Erkkilia et al. 2018) - despite potentially lower CO_2 concentrations in the water column due to daytime photosynthetic uptake. For CH_4, our analyses reveal little difference in day vs. night CH_4 fluxes at FCR.

The discrepancy between the hourly ARIMA results, which identified a strong negative relationship between surface water temperature and hourly GHG fluxes, and the greater daytime EC fluxes of CO_2 may be due to the timing of our day vs. night sampling periods. The hourly ARIMA results imply that cooler temperatures at night are associated with higher CO_2 fluxes, despite overall higher CO_2 fluxes observed in warmer daytime periods. This may be because the mean maximum and minimum surface water temperatures in FCR occurred at 1800 and 0600, respectively, outside of the time periods used to calculate median day (1100 to 1300) and median night (2300 to 0100) fluxes in the diel analysis (Figs. 3, S10). Studies conducted in other lakes found CO_2 flux minima during the late afternoon (~1800) and CO_2 flux maxima during the early morning (~0600; Liu et al. 2016; Shao et al. 2015). Indeed, we found statistically higher CO_2 fluxes measured during dawn (0500 to 0700) as compared to dusk (1700 to 1900), suggesting a close relationship between temperature and CO_2 fluxes, even when outside of the traditional day (noon) versus night (midnight) time periods (Figs. 3, S10).

In addition to water temperature, we also found DO saturation (sat) to be an important predictor for both CO_2 and CH_4 fluxes with negative correlations at the hourly scale. DO sat is an indicator of primary production, with high DO sat associated with high primary production. We hypothesize the negative relationship between DO sat and CO_2 fluxes reflect a weak, but potentially important, role of primary production in constraining fluxes via CO_2 uptake. Previous studies have identified a weak negative relationship between primary production and CO_2 fluxes on the sub-daily timescale in other eutrophic, freshwater lakes and reservoirs; with stronger relationships at longer timescales (Liu et al. 2016; Shao et al. 2015). Other studies have measured high rates of CH_4 oxidation in the surface waters of lakes and reservoirs (Schubert et al. 2012), with positive correlations between DO and CH_4 oxidation rates (Günthel et al. 2019). Thus, unlike for CO_2 where the negative relationship with DO sat is likely an indicator of

584 elevated phytoplankton production, we hypothesize the negative relationship between CH_4 and
585 DO sat on the hourly scale is due to CH_4 oxidation.

586 Our results provide additional evidence that the time of sample collection has important
587 implications for upscaling freshwater GHG fluxes to longer timescales (Attenmeyer et al. 2021;
588 Gómez-Gener et al. 2021). A previous study conducted in FCR which estimated CO_2 and CH_4
589 diffusive fluxes using discrete GHG measurements collected at ~noon, concluded FCR was often
590 a small CO_2 sink during the summer stratified period in 2015-2016 (McClure et al. 2018),
591 whereas our near-continuous EC data indicate that FCR was an overall CO_2 source throughout
592 the summer in 2020. While the flux magnitudes measured by McClure et al. (2018) were similar
593 to the present study, the overall conclusions are different due to the temporal resolution of
594 sample collection. A similar comparison can be found between EC and diffusive fluxes measured
595 during this study, in which higher CO_2 fluxes were observed using the EC system than diffusive
596 fluxes computed from discrete samples for GHG measurements collected only during the day
597 (~noon; Fig. 2). While the discrepancy between day vs. night and dawn vs. dusk fluxes is most
598 evident for CO_2, results from this study suggest we might be missing a key component of CH_4
599 fluxes with only daytime measurements.

600 4.2 Important role of chlorophyll-*a* in constraining daily CO_2 and CH_4 fluxes

601 CWT analysis also identified the daily timescale as an important timescale of variability
602 (Fig. 5). Unlike at the hourly timescale, CO_2 was positively correlated with DO sat and
603 negatively correlated with Chl-*a* at the daily timescale (Table 1). While this result seems
604 counterinitiative, we hypothesize that the magnitude of CO_2 fluxes was greatest on days with
605 high daytime Chl-*a* but low nighttime DO sat due to high respiration. Chl-*a* concentrations were
606 highest in the late-summer and early-fall before and after fall turnover, which corresponded to
607 lower and more variable DO sat (Fig. S2). Conversely, CH_4 fluxes were not correlated with DO
608 sat at the daily scale but were positively associated with Chl-*a*, suggesting higher CH_4 fluxes
609 with higher Chl-*a*. Chl-*a* has been shown to be positively correlated with CH_4 fluxes measured
610 on weekly to twice-weekly timescales, including in FCR (Deemer and Holgerson 2021;
611 DelSontro et al. 2018; McClure et al. 2020). Results here confirm these previous studies but also

612 suggest potentially different controls on CH_4 fluxes on shorter, sub-daily timescales, as discussed
613 above.

614 4.3 Temperature, DO, and fDOM drive weekly to monthly fluxes

615 While several studies have found the sub-daily and daily timescales to be important,
616 comparably fewer studies have investigated longer timescales of variability (weekly to monthly),
617 although these timescales convey important information related to weather patterns and
618 seasonality (Liu et al. 2016; Reed et al. 2018). We found the weekly timescale to be an important
619 timescale of variability for both GHG fluxes (Fig. 5), exclusively during the summer stratified
620 period for CH_4 and in the late spring and summer period for CO_2 (Figs. S8, S9), which may be
621 related to meteorological and limnological (e.g., inflow, primary production) dynamics operating
622 on weekly timescales. At longer timescales, CO_2 and CH_4 flux variability started to diverge, in
623 which the sub-monthly (~20 days) timescale was found to be important for CO_2 while the 6-
624 week timescale (~45 days) was found to be important for CH_4 (Fig. 4). For CO_2, recent studies
625 using EC systems to measure CO_2 fluxes in freshwater systems also found the weekly and
626 monthly timescale to be important, though the mechanisms were not identified (Baldocchi et al.
627 2020; Golub et al. 2021).

628 On weekly to monthly timescales, water temperature was positively associated with both
629 GHG fluxes, as evidenced by higher fluxes in the summer than winter (Fig. 2). Strong
630 correlations between GHG fluxes and temperature have been observed in freshwater ecosystems
631 on longer timescales (monthly to seasonally; Eugster et al. 2011; Reed et al. 2018), largely due to
632 higher rates of primary productivity and microbial respiration under elevated temperature. At the
633 monthly timescale, results suggest that CO_2 fluxes were greatest during months with high
634 primary productivity, as has been observed previously (Liu et al. 2016; Shao et al. 2015). Similar
635 to the daily scale, we hypothesize the negative relationship between DO sat and CH_4 fluxes at the
636 monthly timescale is due to high oxidation rates of CH_4 under high DO sat (Günthel et al. 2019;
637 Schubert et al. 2012).

638 Importantly, fDOM was identified as a key positive environmental predictor for CO_2
639 fluxes at multiple timescales. A similar positive relationship between terrestrially-derived DOM
640 and dissolved CO_2 was identified in 48 Canadian streams (D'Amario and Xenopoulos, 2015). As

fDOM sensors are thought to mainly capture allochthonous DOM (Howard et al. 2021; Watras et al. 2015), this finding suggests that allochthonous DOM from the reservoir's primary inflow steam or diffuse overland flow may result in elevated CO_2 emissions from freshwater ecosystems. This follows previous research which has identified allochthonous carbon inputs and associated DOC concentrations as important predictors of CO_2 fluxes in lakes (Sobek et al. 2005). Unlike for CO_2, fDOM was not identified as an important environmental predictor for CH_4 fluxes at any timescale, suggesting that autochthonous DOM (i.e., derived from primary production) and CH_4 oxidation are likely more important determinants of CH_4 fluxes (Deemer and Holgerson 2021; DelSontro et al. 2018; McClure et al. 2020; Schubert et al. 2012).

4.4 Minimal role of fall turnover and ice cover in affecting GHG dynamics

Contrary to previous studies conducted in both FCR and other thermally-stratified waterbodies (e.g., Erkkilia et al. 2018; McClure et al. 2018; 2020), we observed low CO_2 and CH_4 fluxes during the days surrounding fall turnover (1 November 2020), when EC data indicate that FCR was a small CO_2 source followed by a small CO_2 sink in the days following turnover (Fig. 2). Studies conducted in eutrophic Lake Mendota, USA found similar instances of CO_2 uptake following fall turnover (Baldocchi et al. 2020; Reed et al. 2018); however, unlike FCR, Lake Mendota was a large CO_2 sink throughout the summer stratified period. Discrete diffusive fluxes measured on the day of turnover also suggest FCR was a small CO_2 source (Figs. 2, S4). Similar to CO_2, we found the magnitude of CH_4 fluxes decreased following turnover but remained a small source (Fig. 2). McClure et al. (2018) observed episodic release of CH_4 from FCR on the weeks prior to turnover as high concentrations of CH_4 that had accumulated in the middle of the water column were emitted during storms. In the weeks prior to turnover in this study, we did observe a peak in CH_4 emissions (Figs. 2, S11), supporting this observed mechanism (McClure et al. 2018), and decreasing the importance of fall turnover as a single pulse of emissions.

This study provides some of the first near-continuous flux measurements of both CO_2 and CH_4 during winter (Fig. 4). We found no statistically significant difference between CO_2 or CH_4 fluxes measured during complete ice-off versus partial ice-on, with low fluxes observed during both periods (Fig. 4; Table S8). This lack of difference may be due to emissions occurring from

spatially-heterogeneous sites across the reservoir that exhibited brief ice thaw during the day and refroze at night. Of the few studies that report GHG fluxes during ice-on, all report low fluxes with low variability (Baldocchi et al. 2020; Jammet et al. 2015, 2017; Reed et al. 2018), similar to FCR, although these studies do note high fluxes immediately following ice-off for both CO_2 and CH_4 (Anderson et al. 1999; Baldocchi et al. 2020; Gorsky et al. 2021; Jammet et al. 2015, 2017; Podgrajsek et al. 2015), which was not observed at FCR. Further work on the effect of ice cover on GHG fluxes is needed, but our study suggests that the increasing intermittent and partial ice-cover being experienced in many lakes worldwide (Imrit and Sharma, 2021; Sharma et al. 2021; Woolway et al. 2020) may increase annual GHG fluxes.

4.5 Much higher annual CO_2 emissions from FCR than other studied reservoirs

FCR was a much smaller annual CH_4 source, yet a larger CO_2 source, than other reservoirs reported in the literature to date (Baldocchi et al. 2020; Deemer et al. 2016; Golub et al. 2021). As compared to other reservoirs with GHG flux data, FCR is old (>100 years old) which may lead to lower GHG emissions, particularly CH_4 (Barros et al. 2011; McClure et al. 2020; Prairie et al. 2018). Despite its age, however, FCR is a much larger CO_2 source as compared to other lakes and reservoirs, suggesting emissions may still be high due to mechanisms unexplored in this study.

4.6 Challenges of using EC systems in small, freshwater lakes and reservoirs

While the study described here greatly expands the temporal frequency of measured CO_2 and CH_4 fluxes from a small, eutrophic reservoir, several caveats must be taken into consideration. First, while EC systems greatly expand the temporal resolution of GHG fluxes from freshwater ecosystems, data must be carefully interpreted. EC systems are notoriously difficult to use in freshwater ecosystems due to footprint considerations (Vesala et al. 2006), frequent occurrences of low u_* values, particularly at night (Vesala et al. 2006), as well as general considerations resulting in high percentages of data removed due to these and other issues (yielding data coverage of 10 – 40% prior to gap filling; e.g., Baldocchi et al. 2020; Erkkilia et al. 2018; Houtari et al. 2011; Ouyang et al. 2017; Shao et al. 2015; Waldo et al. 2021; Table S2). These factors can result in relatively sparse data coverage which require gap filling techniques to develop a continuous time-series, as described above, and can increase the

uncertainty of fluxes estimated with the EC system (Baldocchi et al. 2020; Golub et al. 2021; Shao et al. 2015) which were unaccounted for in the current study. Indeed, comparisons between EC measured fluxes and gap-filled fluxes in this study suggest we may be underestimating GHG fluxes from FCR (Fig. S1). In addition, we are unable to rule out potential non-local processes (e.g., land-lake interactions) which occur outside the footprint and are entrained or advected into the EC footprint area (Esters et al. 2020; Vesala et al. 2006, 2011). While these are important considerations, the timeseries of data collected by the EC system is still far more comprehensive than what is possible from discrete measurements (Anderson et al. 1999; Eugster 2003; Houtari et al. 2011; Jonsson et al. 2008) and is needed to increase our understanding of GHG fluxes from small reservoirs on multiple temporal scales.

5 Conclusions

Overall, we observed FCR to be a source of CO_2 and CH_4 to the atmosphere on annual timescales (~600 g CO_2-C m^{-2} yr^{-1}; ~1.0 g CH_4-C m^{-2} yr^{-1}). Importantly, by measuring fluxes near-continuously for a full year, we found winter fluxes of both CO_2 and CH_4 to be comparatively smaller (9.3 and 2.5% of total annual fluxes, respectively) than the summer stratified period yet still important for annual GHG fluxes. Intermittent periods of partial ice-on and ice-off had little effect on either CO_2 and CH_4 fluxes, suggesting that winter fluxes can contribute to annual GHG fluxes from lakes and reservoirs regardless of ice cover. Finally, we identified the importance of both surface water temperature and several other limnological variables (DO sat, Chl-*a*, fDOM), on both CO_2 and CH_4 fluxes on multiple timescales. Altogether, our results suggest that CO_2 and CH_4 are highly dynamic on multiple temporal scales and highlight the role of small reservoirs as important GHG sources in global budgets.

Acknowledgments

This project originated in February 2020 and was made possible through creative teamwork spanning international borders amidst the onset of a global pandemic. We thank Bobbie Niederlehner, Bethany Bookout, Heather Wander, Abigail Lewis, Whitney Woelmer, Dexter

Howard, Nicholas Hammond, Arpita Das, Ryan McClure, Mary Lofton, and Calvin Thomas for their assistance with field collection and laboratory analysis. Zoran Nesic and Vahid Daneshmand provided critical troubleshooting assistance and technical support. Additionally, we thank the Western Virginia Water Authority (WVWA), especially Jamie Morris, for long-term access to field sites and logistical support. We gratefully acknowledge funding from U.S. National Science Foundation grants CNS-1737424, DEB-1753639, DEB-1926050, DBI-1933102, and DBI-1933016; and Fralin Life Sciences Institute at Virginia Tech. We also acknowledge Discovery Grant support to Johnson provided by the Natural Sciences and Engineering Research Council of Canada (NSERC), RGPIN-2020-06252. The authors report no conflicts of interest.

Open Research

The eddy covariance dataset and associated QA/QC code for this study can be found in the Environmental Data Initiative repository via https://doi.org/10.6073/pasta/a1324bcf3e1415268996ba867c636489 (EDI; Carey et al.2022a). Additionally, code used for the timeseries, Morlet wavelet, and ARIMA analyses are archived at https://doi.org/10.5281/zenodo.6093946 (Zenodo; Hounshell et al. 2022). Additional datasets including the meteorological data set (https://portal-s.edirepository.org/nis/mapbrowse?scope=edi&identifier=143&revision=14, Carey et al. 2022c), limnological dataset (https://doi.org/10.6073/pasta/81c6c76f4fe22434a20aa8c00f2d4ad1, Carey et al. 2022d), inflow discharge (https://doi.org/10.6073/pasta/c65755d4c0102dde6e3140c1c91b77d6, Carey et al. 2022e), ice-cover (https://doi.org/10.6073/pasta/a23233527aa90638b2cd3075627c91e6, Carey 2021), and dissolved discrete grab greenhouse gas concentrations (https://doi.org/10.6073/pasta/2fb836492aace4c13b7962f2718be8e5, Carey et al. 2022b) are also archived in the EDI. All published data sets and code are available under the Creative Commons License - Attribution.

References

Anderson, D.E., Striegl, R.G., Stannard, D.I., Michmerhuizen, C.M., McConnaughey, T.A., & LaBaugh, J.W. (1999). Estimating lake-atmosphere CO_2 exchange. *Limnology and Oceanography*, *44*(4), 988–1001. https://doi.org/10.4319/lo.1999.44.4.0988

Attermeyer, K., Casas-Ruiz, J.P., Fuss, T., Pastor, A., Cauvy-Fraunié, S., Sheath, D., et. al. (2021). Carbon dioxide fluxes increase from day to night across European streams. *Communications Earth & Environment*, *2*(1), 118. https://doi.org/10.1038/s43247-021-00192-w

Baldocchi, A.K., Reed, D.E., Loken, L.C., Stanley, E.H., Huerd, H., & Desai, A.R. (2020). *Resolving space and time variation of lake-atmosphere carbon dioxide fluxes using multiple methods* [Preprint]. Biology. https://doi.org/10.1002/essoar.10501554.1

Barros, N., Cole, J.J., Tranvik, L.J., Prairie, Y.T., Bastviken, D., Huszar, V.L.M., del Giorgio, P., & Roland, F. (2011). Carbon emission from hydroelectric reservoirs linked to reservoir age and latitude. *Nature Geoscience*, *4*(9), 593–596. https://doi.org/10.1038/ngeo1211

Bartosiewicz, M., Przytulska, A., Lapierre, J., Laurion, I., Lehmann, M.F., & Maranger, R. (2019). Hot tops, cold bottoms: Synergistic climate warming and shielding effects increase carbon burial in lakes. *Limnology and Oceanography Letters*, *4*(5), 132–144. https://doi.org/10.1002/lol2.10117

Bastviken, D., Sundgren, I., Natchimuthu, S., Reyier, H., & Gålfalk, M. (2015). Technical Note: Cost-efficient approaches to measure carbon dioxide (CO_2) fluxes and concentrations in terrestrial and aquatic environments using mini loggers. *Biogeosciences*, *12*(12), 3849–3859. https://doi.org/10.5194/bg-12-3849-2015

Bastviken, D., Tranvik, L.J., Downing, J.A., Crill, P.M., & Enrich-Prast, A. (2011). Freshwater Methane Emissions Offset the Continental Carbon Sink. *Science*, *331*(6013), 50–50. https://doi.org/10.1126/science.1196808

Beaulieu, J.J., DelSontro, T., & Downing, J.A. (2019). Eutrophication will increase methane emissions from lakes and impoundments during the 21st century. *Nature Communications*, *10*(1), 1375. https://doi.org/10.1038/s41467-019-09100-5

Bunn, A., Korpela, M., Biondi, F., Campelo, F., Mérian, P., Qeadan, F., & Zang, C. (2021, January 31). dplR: Dendrochronology Program Library in R. (Version 1.7.2). [Software]. R Package. https://CRAN.R-project.org/package=dplR

Burnham, K.P., & Anderson, D.R. (2002). *Model selection and multimodel inference: a practical information-theoretic approach*. New York, NY: Springer.

Butman, D., Stackpoole, S., Stets, E., McDonald, C.P., Clow, D.W., & Striegl, R.G. (2016). Aquatic carbon cycling in the conterminous United States and implications for terrestrial carbon accounting. *Proceedings of the National Academy of Sciences*, *113*(1), 58–63. https://doi.org/10.1073/pnas.1512651112

Carey, C.C. (2021). Ice cover data for Falling Creek Reservoir, Vinton, Virginia, USA for 2013-2021. (Version 3). [Dataset]. Environmental Data Initiative (EDI). https://doi.org/10.6073/pasta/a23233527aa90638b2cd3075627c91e6

Carey, C.C., Breef-Pilz, A. & Bookout, B.J. (2022). Time series of high-frequency meteorological data at Falling Creek Reservoir, Virginia, USA 2015-2021 (Version 14). [Dataset]. Environmental Data Initiative (EDI). https://portal-s.edirepository.org/nis/mapbrowse?scope=edi&identifier=143&revision=14

Carey, C.C., Breef-Pilz, A., Hounshell, A.G., Lofton, M.E., McClure, R.P., Gerling, A.B., & Woelmer, W.M. (2022e). Discharge time series for the primary inflow tributary entering Falling Creek Reservoir, Vinton, Virginia, USA 2013-2021. (Version 8). [Dataset]. Environmental Data Initiative (EDI). https://doi.org/10.6073/pasta/c65755d4c0102dde6e3140c1c91b77d6

Carey, C.C., Breef-Pilz, A., Woelmer, W.M., & Bookout, B.J. (2022d). Time series of high-frequency sensor data measuring water temperature, dissolved oxygen, pressure, conductivity, specific conductance, total dissolved solids, chlorophyll a, phycocyanin,

and fluorescent dissolved organic matter at discrete depths in Falling Creek Reservoir, Virginia, USA in 2018-2021. (Version 6). [Dataset]. Environmental Data Initiative (EDI). https://doi.org/10.6073/pasta/81c6c76f4fe22434a20aa8c00f2d4ad1

Carey, C.C., Hanson, P.C., Lathrop, R.C., & St. Amand, A.L. (2016). Using wavelet analyses to examine variability in phytoplankton seasonal succession and annual periodicity. *Journal of Plankton Research*, *38*(1), 27–40. https://doi.org/10.1093/plankt/fbv116

Carey, C.C., Hounshell, A.G., D'Acunha, B.M., Breef-Pilz, A., Thomas, R.Q., & Johnson, M.S. (2022a). Time series of carbon dioxide and methane fluxes measured with eddy covariance for Falling Creek Reservoir in southwestern Virginia, USA during 2020-2022. (Version 1). [Dataset]. Environmental Data Initiative (EDI). https://doi.org/10.6073/pasta/a1324bcf3e1415268996ba867c636489

Carey, C.C., Hounshell, A.G., McClure, R.P., Gerling, A.B., Lewis, A.S.L., & Niederlehner, B.R. (2022b). Time series of dissolved methane and carbon dioxide concentrations for Falling Creek Reservoir and Beaverdam Reservoir in southwestern Virginia, USA during 2015-2021. (Version 6). [Dataset]. Environmental Data Initiative (EDI). https://doi.org/10.6073/pasta/2fb836492aace4c13b7962f2718be8e5

Cole, J.J., & Caraco, N.F. (1998). Atmospheric exchange of carbon dioxide in a low-wind oligotrophic lake measured by the addition of SF_6. *Limnology and Oceanography*, *43*(4), 647–656. https://doi.org/10.4319/lo.1998.43.4.0647

Cole, J.J., Prairie, Y.T., Caraco, N.F., McDowell, W.H., Tranvik, L.J., Striegl, R.G., et. al. (2007). Plumbing the Global Carbon Cycle: Integrating Inland Waters into the Terrestrial Carbon Budget. *Ecosystems*, *10*(1), 172–185. https://doi.org/10.1007/s10021-006-9013-8

Crusius, J., & Wanninkhof, R. (2003). Gas transfer velocities measured at low wind speed over a lake. *Limnology and Oceanography*, *48*(3), 1010–1017. https://doi.org/10.4319/lo.2003.48.3.1010

D'Amario, S.C., & Xenopoulos, M.A. (2015). Linking dissolved carbon dioxide to dissolved organic matter quality in streams. *Biogeochemistry*, *126*(1–2), 99–114. https://doi.org/10.1007/s10533-015-0143-y

Deemer, B.R., Harrison, J.A., Li, S., Beaulieu, J.J., DelSontro, T., Barros, et. al. (2016). Greenhouse Gas Emissions from Reservoir Water Surfaces: A New Global Synthesis. *BioScience*, *66*(11), 949–964. https://doi.org/10.1093/biosci/biw117

Deemer, B.R., & Holgerson, M.A. (2021). Drivers of Methane Flux Differ Between Lakes and Reservoirs, Complicating Global Upscaling Efforts. *Journal of Geophysical Research: Biogeosciences*, *126*(4). https://doi.org/10.1029/2019JG005600

DelSontro, T., del Giorgio, P.A., & Prairie, Y.T. (2018). No Longer a Paradox: The Interaction Between Physical Transport and Biological Processes Explains the Spatial Distribution of Surface Water Methane Within and Across Lakes. *Ecosystems*, *21*(6), 1073–1087. https://doi.org/10.1007/s10021-017-0205-1

Erkkilä, K.M., Ojala, A., Bastviken, D., Biermann, T., Heiskanen, J.J., Lindroth, A., et. al. (2018). Methane and carbon dioxide fluxes over a lake: Comparison between eddy covariance, floating chambers and boundary layer method. *Biogeosciences*, *15*(2), 429–445. https://doi.org/10.5194/bg-15-429-2018

Esters, L., Rutgersson, A., Nilsson, E., & Sahlée, E. (2021). Non-local Impacts on Eddy-Covariance Air–Lake CO_2 Fluxes. *Boundary-Layer Meteorology*, *178*(2), 283–300. https://doi.org/10.1007/s10546-020-00565-2

Eugster, W. (2003). CO_2 exchange between air and water in an Arctic Alaskan and midlatitude Swiss lake: Importance of convective mixing. *Journal of Geophysical Research*, *108*(D12), 4362. https://doi.org/10.1029/2002JD002653

Eugster, W., DelSontro, T., & Sobek, S. (2011). Eddy covariance flux measurements confirm extreme CH₄ emissions from a Swiss hydropower reservoir and resolve their short-term variability. *Biogeosciences*, *8*(9), 2815–2831. https://doi.org/10.5194/bg-8-2815-2011

858 Foken, T., Göockede, M., Mauder, M., Mahrt, L., Amiro, B., & Munger, W. (2004). Post-Field
859 Data Quality Control. In: Lee X., Massman W., Law B. (eds) *Handbook of*
860 *Micrometeorology*. (Vol 29, pp. 181-208). Springer, Dordrecht. https://doi.org/10.1007/1-
861 4020-2265-4_9

862 Gerling, A.B., Munger, Z.W., Doubek, J.P., Hamre, K.D., Gantzer, P.A., Little, J.C., & Carey,
863 C.C. (2016). Whole-Catchment Manipulations of Internal and External Loading Reveal
864 the Sensitivity of a Century-Old Reservoir to Hypoxia. *Ecosystems*, *19*(3), 555–571.
865 https://doi.org/10.1007/s10021-015-9951-0

866 Golub, M., Desai, A.R., Vesala, T., Mammarella, I., Ojala, A., Bohrer, G., et. al. (2021). *New*
867 *insights into diel to interannual variation in carbon dioxide emissions from lakes and*
868 *reservoirs* [Preprint]. Environmental Sciences. https://doi.org/10.1002/essoar.10507313.1

869 Gómez-Gener, L., Rocher-Ros, G., Battin, T., Cohen, M.J., Dalmagro, H.J., Dinsmore, K.J., et.
870 al. (2021). Global carbon dioxide efflux from rivers enhanced by high nocturnal
871 emissions. *Nature Geoscience*, *14*(5), 289–294. https://doi.org/10.1038/s41561-021-
872 00722-3

873 Gorsky, A.L., Lottig, N.R., Stoy, P.C., Desai, A.R., & Dugan, H.A. (2021). The Importance of
874 Spring Mixing in Evaluating Carbon Dioxide and Methane Flux From a Small North-
875 Temperate Lake in Wisconsin, United States. *Journal of Geophysical Research:*
876 *Biogeosciences*, *126*(12). https://doi.org/10.1029/2021JG006537

877 Günthel, M., Donis, D., Kirillin, G., Ionescu, D., Bizic, M., McGinnis, D.F., Grossart, H.P., &
878 Tang, K.W. (2019). Contribution of oxic methane production to surface methane
879 emission in lakes and its global importance. *Nature Communications*, *10*(1), 5497.
880 https://doi.org/10.1038/s41467-019-13320-0

881 Hanson, P.C., Pace, M.L., Carpenter, S.R., Cole, J.J., & Stanley, E.H. (2015). Integrating
882 Landscape Carbon Cycling: Research Needs for Resolving Organic Carbon Budgets of
883 Lakes. *Ecosystems*, *18*(3), 363–375. https://doi.org/10.1007/s10021-014-9826-9

884 Heiskanen, J.J., Mammarella, I., Haapanala, S., Pumpanen, J., Vesala, T., MacIntyre, S., &
885 Ojala, A. (2014). Effects of cooling and internal wave motions on gas transfer
886 coefficients in a boreal lake. *Tellus B: Chemical and Physical Meteorology*, *66*(1), 22827.
887 https://doi.org/10.3402/tellusb.v66.22827

888 Hounshell, A.G. (2022, February 15). aghounshell/EddyFlux: EddyFlux: Hounshell et al. 20XX
889 (Version 1.0.0).[Software] Zenodo. https://doi.org/10.5281/zenodo.6093946

890 Howard, D.W., Hounshell, A.G., Lofton, M.E., Woelmer, W.M., Hanson, P.C., & Carey, C.C.
891 (2021). Variability in fluorescent dissolved organic matter concentrations across diel to
892 seasonal time scales is driven by water temperature and meteorology in a eutrophic
893 reservoir. *Aquatic Sciences*, *83*(2), 30. https://doi.org/10.1007/s00027-021-00784-w

894 Huotari, J., Ojala, A., Peltomaa, E., Nordbo, A., Launiainen, S., Pumpanen, J., et. al. (2011).
895 Long-term direct CO_2 flux measurements over a boreal lake: Five years of eddy
896 covariance data: CO_2 Fluxes of a boreal lake. *Geophysical Research Letters*, *38*(18).
897 https://doi.org/10.1029/2011GL048753

898 Hyndman, R.J. & Athanasopoulos, G. (2018). *Forecasting: principles and practice*, 2nd Edition.
899 Otexts, Melbourne, Australia.

900 Hyndman, R., Athanasopoulos, G., Bergmeir, C., Caceres, G., Chhay, L., O'Hara-Wild, M., et al.
901 (2022, January 10). forecast: Forecasting functions for time series and linear models.
902 (Version 8.16). [Software]. R Package. https://pkg.robjhyndman.com/forecast/

903 Hyndman, R. J., & Khandakar, Y. (2008). Automatic Time Series Forecasting: The **forecast**
904 Package for *R*. *Journal of Statistical Software*, *27*(3).
905 https://doi.org/10.18637/jss.v027.i03

906 Imrit, M.A., & Sharma, S. (2021). Climate Change is Contributing to Faster Rates of Lake Ice
907 Loss in Lakes Around the Northern Hemisphere. *Journal of Geophysical Research:*
908 *Biogeosciences*, *126*(7). https://doi.org/10.1029/2020JG006134

909 Jammet, M., Crill, P., Dengel, S., & Friborg, T. (2015). Large methane emissions from a
910 subarctic lake during spring thaw: Mechanisms and landscape significance: Lake

methane emissions among spring thaw. *Journal of Geophysical Research: Biogeosciences*, *120*(11), 2289–2305. https://doi.org/10.1002/2015JG003137

Jammet, M., Dengel, S., Kettner, E., Parmentier, F.J.W., Wik, M., Crill, P., & Friborg, T. (2017). Year-round CH_4 and CO_2 flux dynamics in two contrasting freshwater ecosystems of the subarctic. *Biogeosciences*, *14*(22), 5189–5216. https://doi.org/10.5194/bg-14-5189-2017

Jonsson, A., Åberg, J., Lindroth, A., & Jansson, M. (2008). Gas transfer rate and CO_2 flux between an unproductive lake and the atmosphere in northern Sweden: CO_2 emission in an unproductive lake. *Journal of Geophysical Research: Biogeosciences*, *113*(G4). https://doi.org/10.1029/2008JG000688

Klaus, M., Seekell, D.A., Lidberg, W., & Karlsson, J. (2019). Evaluations of Climate and Land Management Effects on Lake Carbon Cycling Need to Account for Temporal Variability in CO_2 Concentrations. *Global Biogeochemical Cycles*, *33*(3), 243–265. https://doi.org/10.1029/2018GB005979

Kljun, N., Calanca, P., Rotach, M.W., & Schmid, H.P. (2015). A simple two-dimensional parameterisation for Flux Footprint Prediction (FFP). *Geoscientific Model Development*, *8*(11), 3695–3713. https://doi.org/10.5194/gmd-8-3695-2015

Kljun, N., Rotach, M.W., & Schmid, H.P. (2002). A Three-Dimensional Backward Lagrangian Footprint Model For A Wide Range Of Boundary-Layer Stratifications. *Boundary-Layer Meteorology*, *103*(2), 205–226. https://doi.org/10.1023/A:1014556300021

LiCor Biogeosciences. (2019, December 18). EddyPro® Software (Version 7.0.6) [Software]. LI-COR. https://www.licor.com/env/support/EddyPro/home.html

Liu, H., Zhang, Q., Katul, G.G., Cole, J.J., Chapin, F.S., & MacIntyre, S. (2016). Large CO_2 effluxes at night and during synoptic weather events significantly contribute to CO_2 emissions from a reservoir. *Environmental Research Letters*, *11*(6), 064001. https://doi.org/10.1088/1748-9326/11/6/064001

Lofton, M.E. (2021). melofton/FCR-phytos: Lofton et al. 20XX initial manuscript submission (Version 1.0.0.). [Software]. Zenodo. https://doi.org/10.5281/zenodo.5146268

Loken, L. C., Crawford, J.T., Schramm, P.J., Stadler, P., Desai, A.R., & Stanley, E.H. (2019). Large Spatial and Temporal Variability of Carbon Dioxide and Methane in a Eutrophic Lake. *Journal of Geophysical Research: Biogeosciences*, *124*(7), 2248–2266. https://doi.org/10.1029/2019JG005186

MacIntyre, S., Jonsson, A., Jansson, M., Aberg, J., Turney, D.E., & Miller, S.D. (2010). Buoyancy flux, turbulence, and the gas transfer coefficient in a stratified lake: TURBULENCE AND GAS EVASION IN LAKES. *Geophysical Research Letters*, *37*(24), n/a-n/a. https://doi.org/10.1029/2010GL044164

Mammarella, I., Nordbo, A., Rannik, Ü., Haapanala, S., Levula, J., Laakso, H., et. al. (2015). Carbon dioxide and energy fluxes over a small boreal lake in Southern Finland: CO_2 and Energy Fluxes Over Lake. *Journal of Geophysical Research: Biogeosciences*, *120*(7), 1296–1314. https://doi.org/10.1002/2014JG002873

McClure, R.P., Hamre, K.D., Niederlehner, B.R., Munger, Z.W., Chen, S., Lofton, M.E., Schreiber, M.E., & Carey, C.C. (2018). Metalimnetic oxygen minima alter the vertical profiles of carbon dioxide and methane in a managed freshwater reservoir. *Science of The Total Environment*, *636*, 610–620. https://doi.org/10.1016/j.scitotenv.2018.04.255

McClure, R.P., Schreiber, M.E., Lofton, M.E., Chen, S., Krueger, K.M., & Carey, C.C. (2021). Ecosystem-Scale Oxygen Manipulations Alter Terminal Electron Acceptor Pathways in a Eutrophic Reservoir. *Ecosystems*, *24*(6), 1281–1298. https://doi.org/10.1007/s10021-020-00582-9

Moncrieff, J., Clement, R., Finnigan, J., Meyers, T. (2004). Averaging, Detrending, and Filtering of Eddy Covariance Time Series. In: Lee X., Massman W., Law B. (eds) *Handbook of Micrometeorology*. (Vol 29, pp. 7-31). Springer, Dordrecht. https://doi.org/10.1007/1-4020-2265-4_2

Nyquist, H. (1928). Certain topics in telegraph transmission theory. *Transactions of the American Institute of Electrical Engineers*, *47*, pp. 617–644. https://doi.org/10.1109/T-AIEE.1928.5055024

Ouyang, Z., Shao, C., Chu, H., Becker, R., Bridgeman, T., Stepien, C., John, R., & Chen, J. (2017). The Effect of Algal Blooms on Carbon Emissions in Western Lake Erie: An Integration of Remote Sensing and Eddy Covariance Measurements. *Remote Sensing*, *9*(1), 44. https://doi.org/10.3390/rs9010044

Podgrajsek, E., Sahlée, E., Bastviken, D., Holst, J., Lindroth, A., Tranvik, L., & Rutgersson, A. (2014). Comparison of floating chamber and eddy covariance measurements of lake greenhouse gas fluxes. *Biogeosciences*, *11*(15), 4225–4233. https://doi.org/10.5194/bg-11-4225-2014

Podgrajsek, E., Sahlée, E., Bastviken, D., Natchimuthu, S., Kljun, N., Chmiel, H.E., Klemedtsson, L., & Rutgersson, A. (2016). Methane fluxes from a small boreal lake measured with the eddy covariance method: Methane fluxes from a small boreal lake. *Limnology and Oceanography*, *61*(S1), S41–S50. https://doi.org/10.1002/lno.10245

Prairie, Y.T., Alm, J., Beaulieu, J., Barros, N., Battin, T., Cole, J., et. al. (2018). Greenhouse Gas Emissions from Freshwater Reservoirs: What Does the Atmosphere See? *Ecosystems*, *21*(5), 1058–1071. https://doi.org/10.1007/s10021-017-0198-9

Read, J.S., Hamilton, D.P., Desai, A.R., Rose, K.C., MacIntyre, S., Lenters, J.D., et al. (2012). Lake-size dependency of wind shear and convection as controls on gas exchange: lake-size dependency of u_* and w_*. *Geophysical Research Letters*, *39*(9). https://doi.org/10.1029/2012GL051886

Reed, D.E., Dugan, H.A., Flannery, A.L., & Desai, A.R. (2018). Carbon sink and source dynamics of a eutrophic deep lake using multiple flux observations over multiple years. *Limnology and Oceanography Letters*, *3*(3), 285–292. https://doi.org/10.1002/lol2.10075

Rosentreter, J.A., Borges, A.V., Deemer, B.R., Holgerson, M.A., Liu, S., Song, C., et al. (2021). Half of global methane emissions come from highly variable aquatic ecosystem sources. *Nature Geoscience*, *14*(4), 225–230. https://doi.org/10.1038/s41561-021-00715-2

Schubert, C.J., Diem, T., Eugster W. (2012). Methane emissions from a small wind shielded lake determined by eddy covariance, fluxe chambers, anchored funnels, and boundary model

calculations: A comparison. *Environmental Science & Technology, 46(8),* pp. 4515-4522. https://doi.org/10.1021/es203465x

Shannon, C.E. (1949). Communication in the presence of noise. *Procedings of the IRE, 37(1),* pp. 10–21. https://doi.org/10.1109/JRPROC.1949.232969

Shao, C., Chen, J., Stepien, C.A., Chu, H., Ouyang, Z., Bridgeman, T.B., Czajkowski, K.P., Becker, R.H., & John, R. (2015). Diurnal to annual changes in latent, sensible heat, and CO_2 fluxes over a Laurentian Great Lake: A case study in Western Lake Erie. *Journal of Geophysical Research: Biogeosciences*, *120*(8), 1587–1604. https://doi.org/10.1002/2015JG003025

Sharma, S., Richardson, D.C., Woolway, R.I., Imrit, M.A., Bouffard, D., Blagrave, K., et. al. (2021). Loss of Ice Cover, Shifting Phenology, and More Extreme Events in Northern Hemisphere Lakes. *Journal of Geophysical Research: Biogeosciences*, *126*(10). https://doi.org/10.1029/2021JG006348

Smith, S.V., Renwick, W.H., Bartley, J.D., & Buddemeier, R.W. (2002). Distribution and significance of small, artificial water bodies across the United States landscape. *Science of The Total Environment*, *299*(1–3), 21–36. https://doi.org/10.1016/S0048-9697(02)00222-X

Sobek, S., Tranvik, L.J., & Cole, J.J. (2005). Temperature independence of carbon dioxide supersaturation in global lakes: Carbon dioxide supersaturation in global lakes. *Global Biogeochemical Cycles*, *19*(2),. https://doi.org/10.1029/2004GB002264

Soloviev, A., Donelan, M., Graber, H., Haus, B., & Schlüssel, P. (2007). An approach to estimation of near-surface turbulence and CO2 transfer velocity from remote sensing data. *Journal of Marine Systems*, *66*(1–4), 182–194. https://doi.org/10.1016/j.jmarsys.2006.03.023

Tranvik, L.J., Downing, J.A., Cotner, J.B., Loiselle, S.A., Striegl, R.G., Ballatore, T.J., et. al. (2009). Lakes and reservoirs as regulators of carbon cycling and climate. *Limnology and Oceanography*, *54*(6part2), 2298–2314. https://doi.org/10.4319/lo.2009.54.6_part_2.2298

Torrence, C., & Compo, G.P. (1998). A practical guide to wavelet analysis. *Bulletin of the American Meterological Society, 79(1),* pp.61–78

USACE (United States Army Corps of Engineers). (2021). National inventory of Dams (NID). [accessed 2022 February 7]. https://nid.usace.army.mil/#/

Vachon, D., & Prairie, Y.T. (2013). The ecosystem size and shape dependence of gas transfer velocity versus wind speed relationships in lakes. *Canadian Journal of Fisheries and Aquatic Sciences*, *70*(12), 1757–1764. https://doi.org/10.1139/cjfas-2013-0241

Vesala, T., Eugster, W., & Ojala, A. (2012). Eddy Covariance Measurements over Lakes. In M. Aubinet, T. Vesala, & D. Papale (Eds.), *Eddy Covariance* (pp. 365–376). Springer Netherlands. https://doi.org/10.1007/978-94-007-2351-1_15

Vesala, T., Huotari, J., Rannik, Ü., Suni, T., Smolander, S., Sogachev, A., Launiainen, S., & Ojala, A. (2006). Eddy covariance measurements of carbon exchange and latent and sensible heat fluxes over a boreal lake for a full open-water period. *Journal of Geophysical Research*, *111*(D11), D11101. https://doi.org/10.1029/2005JD006365

Waldo, S., Beaulieu, J.J., Barnett, W., Balz, D. A., Vanni, M.J., Williamson, T., & Walker, J.T. (2021). Temporal trends in methane emissions from a small eutrophic reservoir: The key role of a spring burst. *Biogeosciences*, *18*(19), 5291–5311. https://doi.org/10.5194/bg-18-5291-2021

Watras, C.J., Morrison, K.A., Crawford, J.T., McDonald, C.P., Oliver, S.K., & Hanson, P.C. (2015). Diel cycles in the fluorescence of dissolved organic matter in dystrophic Wisconsin seepage lakes: Implications for carbon turnover: Diel CDOM fluorescence cycles. *Limnology and Oceanography*, *60*(2), 482–496. https://doi.org/10.1002/lno.10026

Wik, M., Thornton, B.F., Bastviken, D., Uhlbäck, J., & Crill, P.M. (2016). Biased sampling of methane release from northern lakes: A problem for extrapolation. *Geophysical Research Letters*, *43*(3), 1256–1262. https://doi.org/10.1002/2015GL066501

Winslow, L. A., Read, J.S., Hanson, P.C., & Stanley, E.H. (2014). Lake shoreline in the contiguous United States: Quantity, distribution and sensitivity to observation resolution. *Freshwater Biology*, *59*(2), 213–223. https://doi.org/10.1111/fwb.12258

Winslow, L., Read, J., Woolway, R., Brentrup, J., Leach T., Zwart, J., Albers, S., & Collinge, C. (2016a, June 9). LakeAnalyzer: Lake Physics Tools. (Version 1.11.4.1). [Software]. R. Package. https://CRAN.R-project.org/package=rLakeAnalyzer

Winslow, L.A., Zwart, J.A., Batt, R.D., Dugan, H.A., Woolway, R.I., Corman, J.R., Hanson, P.C., & Read, J.S. (2016c). LakeMetabolizer: An R package for estimating lake metabolism from free-water oxygen using diverse statistical models. *Inland Waters*, *6*(4), 622–636. https://doi.org/10.1080/IW-6.4.883

Winslow, L., Zwart, J., Batt, R., Corman, J., Dugan, H., Hanson, P., et. al. (2016b, June 23). LakeMetabolizer: Tools for the analysis of ecosystem metabolism. (Version 1.5.0). [Software]. R Package. https://CRAN.R-project.org/pacakge=LakeMetabolizer

Woolway, R.I., Kraemer, B.M., Lenters, J.D., Merchant, C.J., O'Reilly, C.M., & Sharma, S. (2020). Global lake responses to climate change. *Nature Reviews Earth & Environment*, *1*(8), 388–403. https://doi.org/10.1038/s43017-020-0067-5

Wutzler, T., Lucas-Moffat, A., Migliavacca, M., Knauer, J., Sickel, K., Šigut, L., Menzer, O., & Reichstein, M. (2018). Basic and extensible post-processing of eddy covariance flux data with REddyProc. *Biogeosciences*, *15*(16), 5015–5030. https://doi.org/10.5194/bg-15-5015-2018

Wutzler, T., Reichstien, M., Lucas-Moffat, A.M., Menzer, O., Migliavacca, M., & Sickel, K. (2021, December 01). REddyProc: Post Processing of (Half-) Hourly Eddy-Covariance Measurements. (Version 1.3.1). [Software]. R. Package. https://CRAN.R-project.org/package=REddyProc